HHS Public Access

Author manuscript

Sci Signal. Author manuscript; available in PMC 2022 October 05.

Published in final edited form as:

Sci Signal. 2022 April 05; 15(728): eabm2496. doi:10.1126/scisignal.abm2496.

The transcription factor PAX8 promotes angiogenesis in ovarian cancer through interaction with SOX17

Daniele Chaves-Moreira[1], **Marilyn A. Mitchell**[1], **Cristina Arruza**[1], **Priyanka Rawat**[1], **Simone Sidoli**[2,3], **Robbin Nameki**[4,5], **Jessica Reddy**[4,5], **Rosario I. Corona**[4,5], **Lena K. Afeyan**[6,7], **Isaac A. Klein**[6,8,#], **Sisi Ma**[9], **Boris Winterhoff**[10], **Gottfried E. Konecny**[11], **Benjamin A. Garcia**[2], **Donita C. Brady**[12,13], **Kate Lawrenson**[4,14], **Patrice J. Morin**[1], **Ronny Drapkin**[1,*]

[1]Ovarian Cancer Research Center, Department of Obstetrics and Gynecology, University of Pennsylvania Perelman School of Medicine, Biomedical Research Building II/III, Suite 1224, Philadelphia, PA 19104, USA.

[2]Epigenetics Institute, Department of Biochemistry and Biophysics, Smilow Center for Translational Research, University of Pennsylvania Perelman School of Medicine, Suite 9-124, Philadelphia, PA 19104, USA.

[3]Current affiliation: Department of Biochemistry, Albert Einstein College of Medicine, Bronx, NY 10461, USA.

[4]Women's Cancer Research Program at the Samuel Oschin Comprehensive Cancer Center, Cedars-Sinai Medical Center, Los Angeles, CA 90048, USA.

[5]Division of Gynecologic Oncology, Department of Obstetrics and Gynecology, Cedars-Sinai Medical Center, Los Angeles, CA 90048, USA.

[6]Whitehead Institute for Biomedical Research, Cambridge, MA 02142, USA

[7]Department of Biology, Massachusetts Institute of Technology, Cambridge, MA 02142, USA

[8]Department of Medical Oncology, Dana-Farber Cancer Institute, Boston, MA 02215, USA

[9]Institute for Health Informatics, University of Minnesota, MN 55455, USA.

[10]Department of Obstetrics, Gynecology and Women's Health, Division of Gynecologic Oncology, University of Minnesota, Minneapolis, MN 55455, USA.

[*]Corresponding author: rdrapkin@pennmedicine.upenn.edu.

[#]Present address: Dewpoint Therapeutics, Boston MA 02210, USA

AUTHOR CONTRIBUTIONS

DC-M and RD conceived the project and the experimental plan. DC-M, MAM, CA, PR, RN, JR, RIC, LKA, IAK, SM, BW, GEK, DCB, KL, PJM, and RD carried out experiments and analyzed the results. SS and BAG performed and analyzed the mass spectrometry data. DC-M, PJM, and RD drafted the manuscript. All authors provided critical commentary, revisions and reviewed the final manuscript. RD served as overall study supervisor.

COMPETING INTERESTS

G.E. Konecny has served on speaker bureaus for Clovis Oncology, GSK and AstraZeneca and received research funding from Lilly and Merck. I.A.K is now an officer, employee, and shareholder of Dewpoint Therapeutics. R.D. serves on the scientific advisory board of VOC Health and Repare Therapeutics. The other authors declare that they have no potential conflicts of interest.

SUPPLEMENTARY MATERIALS

Figures S1–S6

Tables S1–S2

[11]Department of Medicine, David Geffen School of Medicine, University of California Los Angeles, Los Angeles, CA 90095, USA.

[12]Department of Cancer Biology, University of Pennsylvania Perelman School of Medicine. Biomedical Research Building II/III, Suite 612, Philadelphia, PA 19104, USA.

[13]Abramson Family Cancer Research Institute, University of Pennsylvania Perelman School of Medicine. Biomedical Research Building II/III, Suite 612, Philadelphia, PA 19104, USA.

[14]Center for Bioinformatics and Functional Genomics, Cedars-Sinai Medical Center, Los Angeles, CA 90048, USA.

Abstract

PAX8 is a master transcription factor that is essential during embryogenesis and promotes neoplastic growth. It is expressed by the secretory cells lining the female reproductive tract, and its deletion during development results in atresia of reproductive tract organs. Nearly all ovarian carcinomas express PAX8, and its knockdown results in apoptosis of ovarian cancer cells. To explore the role of PAX8 in these tissues, we purified the PAX8 protein complex from nonmalignant fallopian tube cells and high-grade serous ovarian carcinoma cell lines. We found that PAX8 was a member of a large chromatin remodeling complex and preferentially interacted with SOX17, another developmental transcription factor. Depleting either PAX8 or SOX17 from cancer cells altered the expression of factors involved in angiogenesis and functionally disrupted tubule and capillary formation in cell culture and mouse models. PAX8 and SOX17 in ovarian cancer cells promoted the secretion of angiogenic factors by suppressing the expression of *SERPINE1*, which encodes a proteinase inhibitor with anti-angiogenic effects. The findings reveal a non-cell-autonomous function of these transcription factors in regulating angiogenesis in ovarian cancer.

INTRODUCTION

Epithelial ovarian carcinoma (EOC) is the most lethal of all gynecologic malignancies, annually claiming an estimated 13,000 lives in the United States (1) with worldwide numbers approaching 180,000 deaths yearly (2, 3). The lack of effective screening tools result in the majority of cases being diagnosed at an advanced stage, translating into a 5-year survival rate of less than 30% (4). In addition, EOC has the propensity to acquire chemoresistance and to relapse in most patients, despite initial response to platinum-based chemotherapy after surgical cytoreduction. Although there has been much progress in our understanding of ovarian cancer at the molecular level, targeted therapies have yet to impact overall survival rates (5).

Our understanding of the pathogenesis of high-grade serous ovarian carcinoma (HGSOC), the most common subtype of EOC, has greatly advanced over the past decade. Numerous studies suggest that the fallopian tube secretory epithelial cell (FTSEC) is the cell of origin for the majority of HGSOC (6–15). The development of the fallopian tubes and the rest of the female reproductive tract is governed by the PAX8 transcription factor (16). PAX8 is a member of the Paired-Box (PAX) family of transcription factors that play

essential roles during embryogenesis and tumorigenesis (17, 18). In normal fallopian tubes, PAX8 expression is restricted to the secretory cells; neighboring ciliated cells exhibit no expression. The sustained expression of PAX8 in adult FTSECs and nearly all HGSOCs (19) previously led us to use the *PAX8* promoter to develop a genetically engineered mouse model of HGSOC (20, 21). Knockdown of PAX8 in ovarian cancer cells leads to apoptosis (22–24), supporting a critical role for PAX8 in ovarian cancer growth and progression. Unlike the negligible impact on gene expression in fallopian tube cell lines (24, 25), PAX8 loss in the cancer cell lines alters a considerably high number of transcripts associated with proliferation, angiogenesis, and adhesion pathways (25). Chromatin immunoprecipitation-sequencing (ChIP-seq analysis) had shown that the PAX8 cistrome is reprogrammed during the process of malignant transformation by the widespread redistribution of PAX8 binding sites in the genome of ovarian cancer cells. Moreover, non-coding somatic mutations disrupt the PAX8 transcriptional program in ovarian cancer (26).

To further define the roles of PAX8 in ovarian carcinomas, we purified the PAX8 protein complex from a panel of FTSECs and HGSOC ovarian carcinoma cells, identified its components, and analyzed its biological role. Our findings indicate that PAX8 is part of a chromatin remodeling complex that critically involves SOX17 to promote angiogenesis. Our findings further suggest that targeting this pathway might be a viable therapeutic target in ovarian cancer.

RESULTS

Biochemical purification of the PAX8 complex

To better understand the function of PAX8 in malignant ovarian cancer cells and benign fallopian tube secretory cells, we developed a biochemical affinity-purification method (Fig. 1A). First, we generated nuclear extracts as previously described (27) and purified the endogenous PAX8 protein complex from three ovarian carcinoma cell lines (OVCAR4, KURAMOCHI, and OVSAHO) and three immortalized FTSEC lines (FT194, FT246, and FT282) using PAX8-specific antibodies. Immunoblotting after affinity chromatography demonstrated the specific enrichment of PAX8 in our system (Fig. 1B). When the affinity-purified PAX8 complex was evaluated on size-exclusion chromatography, it revealed a size of approximately 600 kDa (Fig. 1C). Mass spectrometry analysis of the PAX8-containing fractions from the Sephacryl S-300 column identified several putative PAX8-interacting proteins in both normal and cancer cells. Several proteins were common to the PAX8 complexes from normal and cancer cells, with a subset of these proteins present at different levels in these cells (Fig. 1D and Table 1).

Notably, many of the putative PAX8-interacting proteins represent components of chromatin remodeling complexes, including chromodomain-helicase-DNA-binding protein 4 (CHD4), transcriptional repressor p66α (GATAD2A), metastasis-associated protein 2 (MTA2), histone deacetylase 1 (HDAC1), and retinoblastoma binding protein 4 (RBBP4). These proteins are components of the nucleosome remodeling and deacetylase (NuRD) complex, which is responsible for transcriptional repression through histone deacetylation and nucleosome remodeling (28). Some of these proteins (such as HDAC1 and RBBP4) were

found at highly different levels between normal and cancer cells (more than 100-fold; Fig. 1D, Table 1).

To prioritize the putative PAX8-interacting partners for further study, we ranked the peptides by confident identification score (MaxQuant score), correlation with PAX8 expression in ovarian tumor tissues, and co-dependency in ovarian carcinoma cell lines. SOX17, a member of the Sry-related HMG box transcription factor family, exhibited the strongest correlation, co-dependency with PAX8 in ovarian cancer, and was identified among the top-ranked most abundant putative PAX8-interacting partners (Table 1 and fig. S1). We confirmed SOX17 as a *bona fide* PAX8-interacting partner by co-immunoprecipitation using agarose beads covalently bound to either a specific antibody to PAX8 or an antibody to SOX17, compared to rabbit IgG control beads (Fig. 1E), indicating that PAX8 and SOX17 physically interact. In addition, the level of PAX8-SOX17 complexes was markedly increased in HGSOC compared to FTE cells. Consistent with this finding, we observed co-elution of PAX8 and SOX17 in the same large molecular size fractions from the Sephacryl S-300 column (Fig. 1F), indicating that they are part of the same complex. We did not observe monomeric PAX8 or SOX17 in lower molecular weight fractions.

PAX8 physically interacts with SOX17 in HGSOC

We next characterized the location and levels of expression of PAX8 and SOX17 in five normal human fallopian tube tissues and in five different HGSOC cases by immunohistochemistry. In normal tissues, we observed the co-expression of PAX8 and SOX17 in the FT secretory epithelial cells (Fig. 2A). We also observed more abundant expression of both PAX8 and SOX17 in all HGSOC cases (Fig. 2A). Analysis of public datasets in The Cancer Genome Atlas (TCGA) and The Genotype-Tissue Expression (GTEx) portal revealed that PAX8 and SOX17 gene expression levels were significantly higher in ovarian cancers and in benign fallopian tubes than in normal ovaries (fig. S2, A and B).

Our immunohistochemical findings were supported by high-resolution immunofluorescence analyses showing the nuclear co-localization of PAX8 and SOX17 in three different immortalized fallopian tube secretory cell lines (FT194, FT246, and FT282) and three HGSOC cell lines (OVCAR4, KURAMOCHI, and OVSAHO) (Fig. 2B). To visualize the direct interaction of PAX8 and SOX17, we performed an in situ proximity ligation assay (PLA), which enables the identification of both stable and transient protein interactions. We confirmed increased interaction between PAX8 and SOX17 in all the tested HGSOC cell lines: OVCAR4, KURAMOCHI, and OVSAHO (Fig. 2C and fig. S2D). As expected for transcription factors, the observed protein-protein interactions were localized in the nuclei. Moreover, we explored the PAX8-SOX17 interaction in five different HGSOC tissue samples and again we observed a stronger and higher number of PLA signals in the cancer samples than in the normal fallopian tube samples (Fig. 2D), suggesting that the PAX8-SOX17 interaction may be enhanced in the process of malignant transformation. Moreover, in the normal fallopian tube cases, the PLA signals (PAX8-SOX17 interaction) were restricted to the secretory cells, reinforcing the hypothesis that these cells are the site of origin for HGSOC.

Mutual regulation of PAX8 and SOX17

To assess the transcriptional relationship between SOX17 and PAX8, we used RNA interference. Knockdown of PAX8 or SOX17 was achieved with an siRNA pool of four individual siRNAs and confirmed by each siRNA individually. Non-targeting siRNAs served as negative controls. After PAX8 knockdown, SOX17 protein levels were greatly reduced in all tested FTSEC and HGSOC cell lines (Fig. 3, A and B, and fig. S3). Conversely, SOX17 knockdown also led to a decrease in the PAX8 protein level, but the effects were less pronounced. At the RNA level, PAX8 loss led to a significant decline of SOX17 expression in all cell lines studied (Fig. 3C) and SOX17 knockdown similarly led to a decrease of PAX8 expression (Fig. 3D). These data suggest that SOX17 and PAX8 can transcriptionally regulate each other's mRNA expression and that, in the absence of PAX8, SOX17 protein is rapidly depleted.

To determine whether the PAX8-SOX17 complex transcriptionally regulates the *PAX8* and *SOX17* promoters, we performed luciferase reporter assay to directly test the transcriptional effect of this complex on a minimal promoter containing five copies of the PAX8 binding sites (29). Consistent with the results described above, knockdown of either PAX8 or SOX17 demonstrated a significant decline of luciferase activity mediated by PAX8-binding sites (Fig. 3, E and F).

PAX8 and SOX17 regulate a common set of genes

To determine which pathways are regulated by the PAX8-SOX17 complex, we performed RNA sequencing (RNA-seq) in OVCAR4 cells after depletion of each factor individually or after simultaneous depletion of both. Control cells received two independent non-targeting siRNA control pools. The efficiency of the knockdowns was assessed both by the number of sequenced reads, and Western blot. Unsupervised analysis of the significantly altered transcripts after the loss of PAX8, SOX17, or both is shown (Fig. 4A), and the complete list of genes is included in the supplement (table S1). PAX8 target genes were significantly more likely than expected by chance to also be SOX17 target genes ($p<0.00001$, Chi-squared test). PAX8 and SOX17 can both negatively and positively regulate gene expression, although a majority of the significantly altered genes were upregulated following knockdown of PAX8, SOX17, or both. Treatment with siRNAs to simultaneously deplete both factors largely phenocopied the maximal effect of either siPAX8 or siSOX17 (Fig. 4A). We focused on the 380 genes that were commonly up-regulated (Fig. 4B) under all three conditions (absolute log2 fold change ≥ 1, adjusted p-value < 0.05). These genes were enriched in pathways associated with cell adhesion, motility, blood vessel development, and angiogenesis (Fig. 4C).

To further characterize the gene regulation coordinated by PAX8/SOX17, we performed targeted functional proteomic profiling using reverse-phase protein array (RPPA). Knockdown of PAX8, SOX17 or both resulted in significant changes across 142 proteins (p-values < 0.01; Fig. 4D and table S2). Consistent with our observations made using RNA-seq, ontology analysis of the identified target proteins showed that cell adhesion, and angiogenesis were among the pathways most significantly altered after PAX8 and/or SOX17 loss (fig. S4A). When examining individual genes, we found that the gene encoding Serpin

family E member 1 (SERPINE1)—also known as plasminogen activator inhibitor 1 (PAI1) and implicated as an inhibitor of the tissue-type plasminogen activator and angiogenesis (30)—was the most highly increased protein after PAX8/SOX17 knockdowns (Fig. 4E and table S2). The protein data corroborated the RNA-seq analysis, which also found *SERPINE1* mRNA levels as one of the most significantly up-regulated genes following depletion of PAX8, SOX17 or both factors simultaneously by 80 to 95% (fig. S4, B and C). Using immunoblotting and quantitative-PCR, we confirmed that PAX8 or SOX17 knockdown significantly increased the expression of SERPINE1 at both the mRNA and protein level in all tested cell lines (Fig. 4, F and G). Moreover, SERPINE1 presented a strong differential expression pattern between benign and malignant cells. All FTSEC lines exhibited higher levels of SERPINE1 compared to isogenic oncogene-transformed lines or ovarian cancer cell lines (fig. S4C), and this expression was inversely correlated with the levels of PAX8 and SOX17 (fig. S4D). This suggests an important role for PAX8-SOX17-mediated SERPINE1 suppression in malignant transformation. Consistent with these observations, we identified PAX8 and SOX17 binding sites at the *SERPINE1* locus using ChIP-Seq (Fig. 4H) and, using the GeneHancer database (31), we found that these sites are predicted to interact with enhancers associated with the *SERPINE1* promoter.

The angiogenesis regulator, SERPINE1, is regulated by PAX8-SOX17

Using an angiogenesis antibody array, we further examined the levels of 35 different secreted angiogenesis mediators in a panel of human ovarian carcinoma cells (OVCAR3, OVCAR4, KURAMOCHI, and OVTOKO) and a panel of human fallopian tube secretory cells (FT33, FT194, FT246, and FT282). The FTSEC line-conditioned media exhibited a higher concentration of the angiogenesis inhibitors, such as SERPINE1 and THBS1, whereas the ovarian cancer lines secreted more angiogenesis inducers, such as VEGFA, CXCL8, and CXCL16 (Fig. 5A). We found that some angiogenic factors appeared to be regulated by PAX8 and SOX17. The secretion of VEGFA, CXCL8, and CXCL16 were decreased after PAX8 or SOX17 knockdown in the cancer lines, whereas their secretion in the normal lines was not detected (Fig. 5B). However, the most prominent effect observed in cancer cell lines was a large increase in SERPINE1 secretion after PAX8 knockdown (Fig. 5B and fig. S5). Basal SERPINE1 secretion was also increased in FTSECs compared to ovarian cancer lines, with FTSEC-conditioned media containing an average of 20 ng/mL of SERPINE1 compared to an average of 0.2 ng/mL for ovarian cancer cell lines (Fig. 5, C and D). Corroborating our findings, the secretion of SERPINE1 was significantly increased in HGSOC-conditioned media after knockdown of PAX8 or SOX17 (Fig. 5, E and F). Furthermore, analysis of the ovarian cancer samples in the TCGA showed a strong negative correlation between *SOX17* and both *SERPINE1* and *THBS1* (fig. S6).

PAX8 and SOX17 influence angiogenesis through regulation of SERPINE1

Conditioned media from ovarian carcinoma cells induced tube formation by human umbilical vein endothelial cells (HUVECs) in culture, although not to the same extent as in response to recombinant VEGF. This effect was almost abolished in conditioned media from ovarian cancer lines depleted of PAX8 or SOX17 (Fig. 6A). However, no induction of tube formation was observed in HUVECs cultured in conditioned media from FTSEC lines, which exhibit a higher concentration of SERPINE1 (Fig. 6, A and B).

To determine whether the effect of PAX8 and SOX17 on tube-formation is mediated by SERPINE1, we knocked down SERPINE1 in FTSECs and in HGSOC lines, in combination with PAX8 or SOX17 knockdown (Fig. 6C). SERPINE1 knockdown in FTSECs led to a marked increased ability of the conditioned media to induce tube formation, highlighting the important role of this protein in preventing angiogenesis induction by FT cells. PAX8 or SOX17 knockdown did not impair the effects of SERPINE1 knockdown in these cells. In contrast, SERPINE1 knockdown in HGSOC rescued the angiogenesis decrease caused by PAX8 or SOX17 knockdown, indicating that SERPINE1 represents a critical mediator of the effects of these transcription factors on angiogenesis. To confirm these results using an orthogonal assay, we used the spheroid sprouting assay to quantify angiogenesis in a 3-dimensional (3D) microenvironment (Fig. 6D). Consistent with the tube-formation assay, we observed inhibition of sprouting by conditioned media from OVCAR4 upon PAX8 or SOX17 knockdown. However, this inhibition was rescued, at least partially, by the simultaneous knockdown of SERPINE1. Finally, a chemo-invasion assay was performed on these cells to assess the effects of SERPINE1, PAX8 or SOX17 knockdown on the ability of these cells to induce invasion in vascular endothelial cells (Fig. 6E). We observed that SERPINE1 knockdown in FTSEC cells could increase invasion and that this effect could not be reversed by PAX8 or SOX17 knockdown. In HGSOC cells, PAX8 or SOX17 knockdown decreased invasion of vascular endothelial cells, a phenotype partially rescued by SERPINE1 knockdown, again demonstrating the importance of SERPINE1 on the downstream effects of PAX8 and SOX17.

To extend these findings to an in vivo model, we performed the directed in vivo angiogenesis assay (DIVAA) (32, 33) in nude mice. The DIVAA assay uses semi-closed small silicone cylinders (angioreactors), which can be filled with angiogenic or anti-angiogenic compounds of interest. Following subcutaneous implantation in nude mice (Fig. 7A), host vascular endothelial cells will migrate into the angioreactors and proliferate to form new blood vessels if the compound of interest is angiogenic. In the presence of VEGF, used as a positive control, a strong induction of angiogenesis was observed (Fig. 7, A and B). No substantial blood vessels were observed in the vehicle (PBS or fresh medium) control or with SERPINE1. Angioreactors containing OVCAR4-conditioned media revealed extensive angiogenesis, whereas the conditioned media from fallopian tube cells FT194 had no effect. The presence of erythrocytes inside the newly developed blood vessels in OVCAR4 angioreactors indicated that they were functional. In contrast, conditioned media from HGSOC cell lines in which PAX8 or SOX17 was knocked down showed a significant decrease in ovarian cancer-induced neovascularization. These results show that ovarian cancer cell lines have the capacity to induce angiogenesis in vivo, and that PAX8 and SOX17 are crucial in this process (Fig. 7C).

DISCUSSION

Previous studies have shown that benign and malignant cells are distinguished by marked remodeling of the PAX8 cistrome, implying that PAX8 may acquire new targets or functions in the malignant state (25, 34). We analyzed benign and malignant cells to investigate if the PAX8 re-distribution in cancer cells was due to changes in the PAX8 network and to further clarify its roles in ovarian cancer. Its crucial role in transcriptional regulation was

highlighted by our finding that multiple chromatin remodeling proteins interact with PAX8, including several subunits of the NuRD complex CHD4, MTA2, GATAD2A, GATAD2B, HDAC1, and RBBP4. Whereas many of the interacting proteins were present in both benign and malignant PAX8 complexes, their relative abundance differed, highlighting the likely reprogramming of PAX8 previously reported (25, 34) Furthermore, frequent copy number gains at the *PAX8* locus correlate with *PAX8* mRNA levels, and a super-enhancer at the *PAX8* locus likely helps to sustain high-level expression in tumors (35, 36). Acquired somatic mutations within the regulatory elements upstream of PAX8 and within elements bound by PAX8 likely also contribute to dysregulation of PAX8 and target genes in advanced tumors (26). Of note, NuRD complex core members, such as the helicase CHD4, was also found to be an interactor and epigenetic coregulator of PAX3-FOXO1 in alveolar rhabdomyosarcoma (37).

Reinforcing these findings, PAX8 levels are strongly decreased by inhibitors of histone deacetylase 1 (HDAC1) (36). Among the interacting partners identified, SOX17 was one of the mostly highly enriched in our mass spectrometry data. Analysis of TCGA data indicate SOX17 strongly correlates with PAX8 in ovarian cancer, and both genes are frequently amplified in HGSOC, often coincidently. SOX17 is a transcription factor and member of the SOXF family, which has an HMG, β-catenin–binding and transactivation domains (38). Its biological function is dependent on a dimerization partner that is dynamic and specific to the cell context (39). SOX17-interacting partners can engage differentially in the genome, regulating different sets of genes (40). Therefore, we hypothesized that a PAX8-SOX17 transcriptional complex functions in both benign and malignant secretory cells and is important in ovarian tumorigenesis. Our findings concur with the current literature showing that PAX and SOX members can engage in transcriptional regulation. PAX3 and SOX10 can physically interact and synergistically regulate MITF and c-RET enhancers (41). The PAX3-SOX10 interaction is important for melanoma cells, where these factors regulate cell motility, apoptosis, and proliferation (42). Additionally, PAX6 and SOX2 are also interacting partners in early neural differentiation and are necessary for neural progenitor cell pluripotency (43). Furthermore, PAX6 and SOX2 act as an oncogene and can induce cancer cell stemness (44).

We found that PAX8 and SOX17 can mutually regulate each other at the transcriptional level. At the protein level, PAX8 knockdown led to an almost complete disappearance of SOX17, and SOX17 knockdown led to a substantial decrease in PAX8 levels. These results are consistent with our previously reported findings that PAX8 and SOX17 are master transcription factors that occupy regulatory elements related to their own encoding genes in ovarian cancer (45). Globally, PAX8 and SOX17 genomic binding sites co-localize within candidate active enhancers in HGSOC cell lines. In addition, PAX8 binds near the *SOX17* gene locus, which confirms the co-regulation observed in SOX17 transcript and protein levels (45). Our transcriptomic and proteomic analyses revealed that PAX8 and SOX17 commonly regulate a family of genes associated with blood vessel formation, suggesting a cooperative role in orchestrating an important pro-angiogenic transcriptional program in ovarian cancer. In this setting, it may be interesting to note that SOX17 was found overexpressed in highly vascularized human glioblastoma and that murine Sox17 can promote tumor angiogenesis (46).

Our analysis of PAX8/SOX17-target genes revealed SERPINE1 to be the most highly and commonly up-regulated both at the transcript and protein levels. SERPINE1 is a serine proteinase inhibitor, belonging to the Serpin family, which is an important endothelial plasminogen activator inhibitor and urokinase inhibitor (47). Important roles in coagulation, extracellular matrix remodeling, and angiogenesis have been reported for SERPINE1. The anti-angiogenic effects of SERPINE1 seem to be mediated by binding to vitronectin and blocking integrin αvβ3 and uPAR binding sites (48). Therefore, binding of secreted SERPINE1 to vitronectin blocks cell adhesion, migration, and inhibits angiogenesis (49). Moreover, SERPINE1 can inhibit VEGFR-2 activation by blocking the pro-angiogenic binding interaction between VEGFR-2 and integrin αVβ3 (50). Therefore, this regulation of the VEGF pathway by SERPINE1 is notable, as VEGF is a potent mediator of tumor angiogenesis in various tumors, and ovarian cancer patients with high levels of VEGF have been reported to have worse prognoses and lower survival rates. It is important to note that SERPINE1 has been reported to have both pro- and antiangiogenic function, with the amounts of SERPINE1 being a major determinant in these effects (47). Our results show that in ovarian cells, SERPINE1 is an essential inhibitor of tumor angiogenesis, which is downregulated upon activation of PAX8-SOX17 signaling. Based on these experiments, we hypothesize that suppressing SERPINE1 through malignant transformation, triggers VEGF pathway activation in vivo and contributes to tumor angiogenesis (Fig. 7C).

Our results may also help explain some of the developmental defects described in the *Pax8* knockout mouse (16). *Pax8*$^{-/-}$ mice are infertile because they lack a functional uterus revealing only remnants of myometrial tissue. In addition, the vaginal opening is absent. Folliculogenesis, ovarian hormone production, and transcription of pituitary hormones are in a normal range. Thus, infertility in *Pax8*$^{-/-}$ mice seems to be due to a defect in development of the reproductive tract rather than to hormonal imbalance, pointing to a direct morphogenic role for PAX8 in uterine development. Our observation that PAX8 and SOX17 orchestrate an angiogenic program may help explain the atresia of the reproductive tract seen in the *Pax8*$^{-/-}$ mice. The absence of Pax8 in the developing reproductive tract is likely accompanied by low SOX17 and high SERPINE1. These conditions would effectively shut down blood vessel development and prevent the development of the organ. This is reminiscent of the severe embryopathy seen with thalidomide in the early 1960s (51). Thalidomide was marketed as an anti-emetic which was later shown to have anti-angiogenic properties that cause severe birth defects, including phocomelia (limb defects), genital, and internal organ absence or malformation.

Current evidence supports a model by which various PAX8 interactions will control different cellular functions (18). For example, the interaction between PAX8 and MECOM is crucial in cell adhesion and cellular matrix regulation in ovarian cancer (52). Here, we have shown that PAX8 physically interacts with SOX17 in FTSEC and HGSOC, leading to changes in multiple transcriptional programs, including modulation of genes mediating tumor angiogenesis. Using in vitro and in vivo angiogenesis assays, we demonstrated that PAX8/SOX17 can regulate angiogenesis during tumor development, and that SERPINE1 is a crucial mediator of this effect. Overall, our work suggests that inhibition of the PAX8/SOX17 pathway may be of potential value as part of an anti-angiogenic approach to the treatment of ovarian cancer.

MATERIALS AND METHODS

Cells and Tissues

Human immortalized fallopian tube secretory cells (FT33, FT194, FT246, FT282 and FT282-E) were maintained in standard conditions as previously described (53) and grown in DMEM/F12 containing 2% Ultroser-G serum substitute. OVCAR3 was obtained from ATCC, OVCAR4 was acquired from William C. Hahn's lab-CCLE (Dana-Farber Cancer Institute), JHOS2 was from Gottfried Konecny (University of California Los Angeles), and KURAMOCHI, OVSAHO, and OVTOKO were obtained from JCRB Cell Bank (Japan). All lines were maintained as recommended by supplier. The human umbilical vein endothelial cells (HUVEC) were acquired from Sigma-Aldrich and maintained according to manufacturer instructions. All cell lines were sent to the Wistar Institute Genomic Core Facility for authentication using short tandem repeat profiling and for detection of *Corynebacterium bovis* infection. In addition, all cell lines were also tested for *Mycoplasma* sp. at the University of Pennsylvania Cell Center.

Following approval by the Hospital of Pennsylvania Institutional Review Board, we obtained human fallopian tube and human high-grade serous ovarian carcinoma formalin-fixed and paraffin-embedded sections from the Department of Pathology at Hospital of the University of Pennsylvania to evaluate the expression of PAX8 and SOX17.

Purification of endogenous PAX8

Benign and malignant cells were grown in 15-cm plates until 90% confluence, washed twice with PBS, trypsinized, neutralized and collected. Nuclear fractionation was prepared as previously published (27). Harvested cells were resuspended in hypotonic buffer [20 mM HEPES, pH 7.5, 10 mM KCl, 1 mM EDTA, 1 mM EGTA, 1.5 mM $MgCl_2$, 2 mM dithiothreitol, protease inhibitors (Sigma-Aldrich: P8340), and phosphatase inhibitors (Sigma-Aldrich: P5726)] and incubated for 30 minutes. Samples were then disrupted through a 22G needle and centrifuged at 10,000 × *g* for 10 minutes at 4°C. Nuclei-enriched fraction was sonicated with complete RIPA buffer (Cell Signaling Technology: 9806S) containing protease inhibitors (Sigma-Aldrich: P8340), and phosphatase inhibitors (Sigma-Aldrich: P5726), and spun down for 10 minutes at 10,000 × g at 4°C. The supernatant (500 μg of nuclear extract) was incubated for 16 hours at 4°C with 105 μg of PAX8-specific antibody (Proteintech: 10336-1-AP) coupled to 1 ml of Protein A agarose resin (Thermo-Fisher: 44893) or with 105 μg of normal rabbit IgG (Proteintech: 30000-0-A) coupled to 1 mL of Protein A agarose resin, as negative control. The columns were washed three times with 10 mL of 0.1 M phosphate and 0.15 M NaCl, pH 7.2 and eluted with 0.5 M NaCl and 0.1 M glycine, pH 2.8. Fractions had their pH equilibrated with 1M Tris, pH 9.5, separated by gel electrophoresis, Coomassie blue-stained and lanes were sent for mass spectrometry analysis.

The affinity column eluates containing PAX8 were also loaded onto a 100 ml Sephacryl S-300 column (Sigma-Aldrich: S300HR-100ML) equilibrated with 50mM Tris, pH 7.5, 100 mM KCL, 0.5 M NaCl, 1% NP-40 and 1% glycerol. We collected one hundred and fifty 500 μL fractions and protein peaks were separated by gel electrophoresis, silver-stained

(Thermo-Fisher: 24600), checked by Western blots for the presence of PAX8, and PAX8-positive fractions were also submitted for mass spectrometry analysis.

Identification of PAX8 interacting partners

Coomassie blue-stained lanes containing PAX8 were analyzed by nanoLC-MS/MS setup as previously described (54). In summary, HPLC gradient was set between 0–30% of solvent A = 0.1% formic acid and solvent B = 95% acetonitrile, 0.1% formic acid for one hour followed by five minutes of 30% to 85% of solvent B and ten minutes of isocratic 85% solvent B. Flow rate of nLC was set to 300 nL/min and coupled to Orbitrap Fusion Tribrid mass spectrometer (Thermo Fisher, USA) with 2.5 kV spray voltage and 275 °C of capillary temperature. Full mass spectrometry was performed using a resolution of 120,000 and 27 of HCD. DDA files were analyzed with MaxQuant (55) using a SwissProt human database. iBAQ quantification was used for enrichment analysis and data were log2 transformed and normalized by subtracting the average of all valid values for each sample. Statistics analysis was obtained applying a two-tails heteroscedastic t-test.

TCGA and GTEx expression analysis

RNA-Seq data from TCGA and GTEx were retrieved using databank links (https://xenabrowser.net/ and https://gtexportal.org/home/). From the available data types, gene expression was selected for Fallopian tube (FT), Ovary (OV), Serous Ovarian Carcinoma (SOC), and TCGA Ovarian Cancer (TCGA-OV). Using GraphPad Prism unpaired t-test PAX8 and SOX17 expression was analyzed and adjusted P-value <0.001 were reported as statistically significant.

protein-protein interaction analysis in situ

Prior to the protein-protein interaction staining by in situ proximity ligation assay (PLA), tissue sections and cell lines were processed as described in the IHC and IF sections. PLA signals were determined employing Duolink Probes Anti-Mouse MINUS (Sigma-Aldrich; DUO92004) and Anti-Rabbit PLUS (Sigma-Aldrich; DUO92002) according to the manufacturer's recommended protocol following overnight incubation with anti- antibody to mouse PAX8 at 1:250 (Novus; NBP2-29903) and to rabbit SOX17 at 1:250 (Cell Signaling Technology; 81778S) at 4 °C. Red fluorescent signals were obtained using detection reagent red (Sigma-Aldrich: DUO92008) and chromogen signals was acquired using detection reagent brightfield (Sigma-Aldrich; DUO92012).

siRNA knockdown

All knockdowns were performed by reverse transfection using a pool of four siRNAs that were individually deconvoluted and validated. Fallopian tube secretory cells (300,000) or ovarian carcinoma cells (300,000) were incubated with 10 μl of Lipofectamine RNAiMax (Thermo-Fisher: 13778075), and 30 nM of the respective siRNA [(ON-TARGETplus Human PAX8 siRNA (Dharmacon:L-003778-00-0005), ON-TARGETplus Human SOX17 siRNA (Dharmacon: L-013028-01-0005) or non-targeting siRNA as negative control (Dharmacon: D-001810-10-05)] in Opti-MEM reduced serum medium (Gibco: 31985088) as recommended by the manufacturer's protocol.

Immunohistochemistry

Fallopian tube and high-grade ovarian carcinoma sections were processed as previously reported (55). The immunohistochemical staining were performed using a dilution of 1:500 of antibodies to PAX8 (Novus: NBP1-32440) or SOX17 (Novus: NBP1-47996). Slides were scanned with Aperio CS2.

Immunofluorescence

10^4 cells from each FTSEC and HGSOC line were seeded onto imaging plates (Eppendorf: 0030741030) and allowed to grow for 24 hours. Cells were washed twice in PBS, and fixation was performed for 15 min with paraformaldehyde 4% (Thermo-Fisher: AAJ19943K2) at room temperature. Cells were then washed twice in PBS and permeabilized with Triton X-100 0.25% (Boston BioProducts: P-924) for 15 min. Aldehyde residues were quenched with glycine 100 mM (Sigma-Aldrich: 50046-50G) for 15 min. The unspecific sites were blocked with a solution of 1% bovine serum albumin, and 0.1% Tween 20 in PBS for 30 min. Samples were incubated for 16 hours at 4 °C with a dilution of 1:500 of antibody to PAX8 (Novus: NBP1-32440) or SOX17 (Novus: NBP1-47996). Cells were then washed three times for 5 min each in a solution of 1% bovine serum albumin and 0.1% Tween 20 in PBS followed by incubation for one hour with AlexaFluor488-conjugated anti-mouse IgG antibody or AlexaFluor594-conjugated anti-rabbit IgG antibody. Cells were washed three times in PBS, mounted in Fluoromount-G with DAPI, and images were acquired at 60X magnification with a Nikon Eclipse Ti inverted microscope.

Western blot analysis

Samples were incubated with RIPA buffer (Cell Signaling Technology: 9806S) for 30 min at 4°C followed by centrifugation at 10,000 × g for 5 min. Supernatants' protein concentration was estimated by BCA method (Thermo-Fisher: 23227). Thirty micrograms of each sample were mix with sample buffer loaded and separated using Mini-PROTEAN TGX 4–15% polyacrylamide gels (BioRad: 4561083) and Tris/Glycine/SDS buffer (BioRad: 1610732). TURBO transfer system (BioRad: 1704156) was employed to move separated samples from gels to PVDF membranes. Primary antibodies to PAX8 (Novus: NBP1-32440), SOX17 (Abcam: ab224637) and GAPDH (Cell Signaling Technology: 5174) were diluted 1:1000 in 5% nonfat milk in TBS containing 0.1% Tween 20 and incubated with the membranes overnight at 4°C. Membranes were then washed three times in TBS containing 0.1% Tween 20 then incubated with HRP-conjugated anti-rabbit IgG antibody (Cell Signaling Technology: 7074). Images were acquired by chemiluminescence using Clarity ECL (BioRad: 1705062).

Co-immunoprecipitation

500 μg of nuclear lysates were incubated with 25 μg of a specific PAX8 antibody (Novus: NBP1-32440), 25 μg of a specific SOX17 antibody (Abcam: ab224637), or 25 μg of a normal rabbit IgG (Cell Signaling Technology: 2729S) covalently coupled to activated agarose beads (Thermo-Fisher: 26148) as manufacturer's recommended protocol.

RNA sequencing

Transcriptome analysis of OVCAR4 cells after PAX8, SOX17, or simultaneous knockdown has been described previously (56). Briefly, ovarian carcinoma cells had their RNA chemically purified using the Nucleospin RNA Plus kit (Macherey-Nagel: 740984.50) as recommended by the manufacturer's protocol. Poly-A non-stranded library were prepared using the newly extracted RNA and forty million reads were sequenced by BGI platform. Bioinformatic analyses were executed employing the R package DESeq2 (version 1.24.0). Significant changes were designated as log2 fold change ≥ 1 and adjusted *P*-value ≤ 0.01. Metascape tool was employed to identify the differentially enriched pathways.

Conditioned medium

Secretory cells and carcinoma cells were growth in 60 mm dish at 37 °C and 5% CO2. Conditioned media were retrieved by spinning down at 2,000 × g for 5 min at 4 °C then supernatants were passed through 0.22 μm filter (Millipore: SLGP033RS).

Angiogenesis array and ELISA

Secreted angiogenesis mediators were identified in fallopian tube secretory cell and ovarian carcinoma cell conditioned media using the Human Angiogenesis Antibody Array (R&D systems: ARY007). ELISAs was employed for the precise quantification of VEGF (R&D systems: DVE00) and SERPINE1 (R&D systems: DSE100) from conditioned media as recommended by the manufacturer's protocol. Fresh DMEM/F12 or RMPI media were tested and used as a negative control.

Gene-specific occupancy by PAX8 and SOX17 using ChIP-Seq analysis

We analyzed our previously reported ChIP-Seq data for SOX17 and PAX8 (45) for binding of these transcription factors in the proximity of SERPINE1, and enhancer interactions were predicted using the GeneHancer database (31).

Tube formation assay

Twenty thousand HUVEC cells were seeded in reduced growth factor basement membrane extract (BME)-coated 96-well plates (R&D systems: 3470-096-K). Endothelial cells were exposed to 100 μl of the different benign or malignant cells conditioned media, 10 ng/ml VEGF (R&D systems: 293-VE-010) or 10 μg/ml SERPINE1 (R&D systems: 1786-PI-010) for 6 hours at 37 °C. HUVEC cells were labeled with 2 μM Calcein AM as recommended by the manufacturer's protocol to facilitate the image acquisition using a Nikon Eclipse Ti inverted microscope. The number of complete endothelial loops per field were counted and compared.

Sprouting assay

Microfluidic plates (Mimetas: 4003-400B) were used for the 3D endothelial sprouting assay as previous described (60). Briefly, collagen type I (R&D systems: 3447-020-01) was used as the 3D scaffold. After incubation for solidification, the plate was removed from the incubator and kept sterile at room temperature before cell loading. Endothelial cells were dissociated, pelleted, and suspended in basal medium at a concentration of 2×10^7 cells/mL.

2 μL of the cell suspension was dispensed into the perfusion inlet and incubated for 45 min at 37 °C, 5% CO2. After the cells attached to the bottom of the perfusion channel, 50 μL of medium was added in the perfusion inlet and outlet wells and the plates were placed on a rocker platform for continuous perfusion. (Perfusion rocker, MIMETAS). Medium was refreshed three times a week. Angiogenic sprouting were stimulated with a combination of VEGF, FGF, PMA, and S1P (Positive Control), basal medium (Negative Control), or OVCAR4 conditioned media after each specific knockdown for 7 days.

Invasion assay

The endothelial cell invasion was performed accordingly to the manufacturer's recommendation (Trevigen: 3471-096-K). Using 96 wells invasion chambers, 50 μl of cell suspension (20,000 cells) were added per well to top chamber upon 0.1X BME Coating Solution. Angiogenic mediators (VEGF or SERPINE1), basal media, or conditioned media after knockdowns were added to the bottom chamber and incubated for 24 hours. The detection of cell invasion was quantified using the Calcein-AM internalized by the endothelial cells.

In vivo angiogenesis assay

Following IACUC review and approval (Protocol #806687), directed in vivo angiogenesis assays (DIVAA) (R&D systems: 3450-048-K) were performed as recommended by the manufacturer's protocol. Briefly, six-week-old female nude mice (JAX: 002019) were kept in aseptic conditions under the Stem Cell and Xenograft Core barrier at the University of Pennsylvania. Mice cohorts were anesthetized with 2% isoflurane prior the subcutaneously implantation of angioreactors, meaning a 1cm flexible silicone cylinder. Dorsal-lateral incisions were made on each nude mouse, wherein angioreactors filled with FTSEC- or HGSOC-conditioned media, 10 ng/ml VEGF (R&D systems: 293-VE-010), or 10 μg/ml SERPINE1 (R&D systems: 1786-PI-010) were subcutaneously inserted under the skin and then sutured to cover the incisions. Angioreactors were retrieved after 14 days of incubation for careful collection of the mouse endothelial cells that were attracted and invaded the cylinders. Neovascularization was quantified by staining the endothelial cells with FITC-lectin and measuring the intensity of fluorescence within a Thermo-Fisher Fluoroskan Ascent FL fluorimeter at 485nm. The animals' care and experimentation were performed under approved protocols and were in accordance with institutional guidelines.

Real-time PCR

Samples total RNA was purified using the RNeasy Plus Mini Kit (Qiagen: 74134), quantified and used as a template for the synthesis of single-stranded cDNA employing the High -Capacity cDNA Reverse Transcription Kit (Thermo-Fisher: 4374966). To access the gene expression changes we employed the TaqMan Assay (Thermo-Fisher: 4331182) using 100 ng of cDNA per 20 μL of final reaction with TaqMan Fast Advanced Master Mix (Thermo-Fisher: 4444557) as recommended in the manufacturer's protocol.

Reverse-phase protein array (RPPA)

Arrays were performed at the Department of Bioinformatics and Computational Biology at MD Anderson Cancer Center as previously described (57, 58). The platforms contain over 300 antibodies exclusively validated with a Pearson coefficient > 0.7 of correlation between RPPA and WB were employed in the proteomic analysis (59). Spots intensities were generated by colorimetric reaction employing the Dako Cytomation-Catalyzed System.

Luciferase reporter assay

Briefly, half-million cells were co-transfected with 1 μg of PAX8-(Firefly) Luciferase reporter vector (28), 0.5 μg of CMV-(*Renilla*) Luciferase control vector (Promega: E2261) and 30 nM of PAX8, SOX17 or non-targeting siRNA, using Lipofectamine 2000 (Thermo-Fisher: 11668027) as recommended by manufacturer's protocol. Plates containing the different transfected cells were incubated for 24 hours at 37°C before the luciferase activity was measured using the Dual-Glo luciferase detection kit (Promega: E2920).

Statistical analysis

Representative graphics are displayed as mean and standard derivation of experiments replicates. Significant changes $P < 0.05$ between controls and knockdowns were acquired applying ANOVA and Student's tests (GraphPad Prims 8).

Supplementary Material

Refer to Web version on PubMed Central for supplementary material.

ACKNOWLEDGMENTS

We thank Drs. Kai Doberstein and Richard Young for support and critical reading of the manuscript. We appreciate members of the Drapkin laboratory for helpful suggestions and discussions. We are grateful to Cynthia Lopez-Haber for her technical insights, Gregory Dressler for sharing the PAX8-Luciferase reporter vector, and Andrew Kung for donating the FUW-Luc-mCherry vector. In addition, we are very grateful for the Penn Stem Cell & Xenograft Core, the Penn Quantitative Proteomics Resource Core, and the MD Anderson RPPA Core (NCI P30 CA16672) for technical assistance and resource access. We are also very appreciative of Tony Secreto and Lauren Schwartz support and expertise.

FUNDING

This work was supported by an NIH SPORE in ovarian cancer P50 CA228991 (R.D.), the Dr. Miriam and Sheldon G. Adelson Medical Research Foundation (R.D.), the Honorable Tina Brozman Foundation for Ovarian Cancer Research (R.D.), the Basser Center for BRCA (R.D.), the Claneil Foundation (R.D.), an NIH P01CA196539 (B.A.G), the Ann and Sol Schreiber Mentored Investigator Award (545754) from the Ovarian Cancer Research Alliance (D. C-M), the Liz Tilberis Early Career Award (599175), also from the Ovarian Cancer Research Alliance (K.L.), and a Research Scholars Grant from the American Cancer Society (K.L.).

DATA AND MATERIALS AVAILABILITY

The RNAseq dataset (GSE151316) and the ChIP-Seq dataset (GSE152885) have been deposited in GEO. The mass spectrometry raw files are publicly available in the repository Chorus at the project number 1755. All other data needed to evaluate the conclusions in the paper are present in the paper or the Supplementary Materials.

REFERENCES AND NOTES

1. Siegel RL, Miller KD, Fuchs HE, Jemal A, Cancer statistics, 2022. CA Cancer J Clin 72, 7–33 (2022); published online EpubJan (10.3322/caac.21708). [PubMed: 35020204]
2. Ferlay J, Colombet M, Soerjomataram I, Mathers C, Parkin DM, Pineros M, Znaor A, Bray F, Estimating the global cancer incidence and mortality in 2018: GLOBOCAN sources and methods. Int J Cancer 144, 1941–1953 (2019); published online EpubApr 15 (10.1002/ijc.31937). [PubMed: 30350310]
3. Zheng L, Cui C, Shi O, Lu X, Li YK, Wang W, Li Y, Wang Q, Incidence and mortality of ovarian cancer at the global, regional, and national levels, 1990–2017. Gynecol Oncol 159, 239–247 (2020); published online EpubOct (10.1016/j.ygyno.2020.07.008). [PubMed: 32690392]
4. Reid BM, Permuth JB, Sellers TA, Epidemiology of ovarian cancer: a review. Cancer Biol Med 14, 9–32 (2017); published online EpubFeb (10.20892/j.issn.2095-3941.2016.0084). [PubMed: 28443200]
5. Torre LA, Trabert B, DeSantis CE, Miller KD, Samimi G, Runowicz CD, Gaudet MM, Jemal A, Siegel RL, Ovarian cancer statistics, 2018. CA Cancer J Clin 68, 284–296 (2018); published online EpubJul (10.3322/caac.21456). [PubMed: 29809280]
6. Perets R, Drapkin R, It's Totally Tubular....Riding The New Wave of Ovarian Cancer Research. Cancer Res 76, 10–17 (2016); published online EpubJan 1 (10.1158/0008-5472.CAN-15-1382). [PubMed: 26669862]
7. Ducie J, Dao F, Considine M, Olvera N, Shaw PA, Kurman RJ, Shih IM, Soslow RA, Cope L, Levine DA, Molecular analysis of high-grade serous ovarian carcinoma with and without associated serous tubal intra-epithelial carcinoma. Nat Commun 8, 990 (2017); published online EpubOct 17 (10.1038/s41467-017-01217-9). [PubMed: 29042553]
8. Labidi-Galy SI, Papp E, Hallberg D, Niknafs N, Adleff V, Noe M, Bhattacharya R, Novak M, Jones S, Phallen J, Hruban CA, Hirsch MS, Lin DI, Schwartz L, Maire CL, Tille JC, Bowden M, Ayhan A, Wood LD, Scharpf RB, Kurman R, Wang TL, Shih IM, Karchin R, Drapkin R, Velculescu VE, High grade serous ovarian carcinomas originate in the fallopian tube. Nat Commun 8, 1093 (2017); published online EpubOct 23 (10.1038/s41467-017-00962-1). [PubMed: 29061967]
9. Wu RC, Wang P, Lin SF, Zhang M, Song Q, Chu T, Wang BG, Kurman RJ, Vang R, Kinzler K, Tomasetti C, Jiao Y, Shih IM, Wang TL, Genomic landscape and evolutionary trajectories of ovarian cancer precursor lesions. J Pathol 248, 41–50 (2019); published online EpubMay (10.1002/path.5219). [PubMed: 30560554]
10. Eckert MA, Pan S, Hernandez KM, Loth RM, Andrade J, Volchenboum SL, Faber P, Montag A, Lastra R, Peter ME, Yamada SD, Lengyel E, Genomics of Ovarian Cancer Progression Reveals Diverse Metastatic Trajectories Including Intraepithelial Metastasis to the Fallopian Tube. Cancer Discov 6, 1342–1351 (2016); published online EpubDec (10.1158/2159-8290.CD-16-0607). [PubMed: 27856443]
11. Sherman-Baust CA, Kuhn E, Valle BL, Shih Ie M, Kurman RJ, Wang TL, Amano T, Ko MS, Miyoshi I, Araki Y, Lehrmann E, Zhang Y, Becker KG, Morin PJ, A genetically engineered ovarian cancer mouse model based on fallopian tube transformation mimics human high-grade serous carcinoma development. J Pathol 233, 228–237 (2014); published online EpubJul (10.1002/path.4353). [PubMed: 24652535]
12. McCool KW, Freeman ZT, Zhai Y, Wu R, Hu K, Liu CJ, Tomlins SA, Fearon ER, Magnuson B, Kuick R, Cho KR, Murine Oviductal High-Grade Serous Carcinomas Mirror the Genomic Alterations, Gene Expression Profiles, and Immune Microenvironment of Their Human Counterparts. Cancer Res 80, 877–889 (2020); published online EpubFeb 15 (10.1158/0008-5472.CAN-19-2558). [PubMed: 31806642]
13. Kim J, Coffey DM, Creighton CJ, Yu Z, Hawkins SM, Matzuk MM, High-grade serous ovarian cancer arises from fallopian tube in a mouse model. Proc Natl Acad Sci U S A 109, 3921–3926 (2012); published online EpubMar 6 (10.1073/pnas.1117135109). [PubMed: 22331912]
14. Stuckelberger S, Drapkin R, Precious GEMMs: emergence of faithful models for ovarian cancer research. J Pathol 245, 129–131 (2018); published online EpubJun (10.1002/path.5065). [PubMed: 29493783]

15. Dinh HQ, Lin X, Abbasi F, Nameki R, Haro M, Olingy CE, Chang H, Hernandez L, Gayther SA, Wright KN, Aspuria PJ, Karlan BY, Corona RI, Li A, Rimel BJ, Siedhoff MT, Medeiros F, Lawrenson K, Single-cell transcriptomics identifies gene expression networks driving differentiation and tumorigenesis in the human fallopian tube. Cell Rep 35, 108978 (2021); published online EpubApr 13 (10.1016/j.celrep.2021.108978). [PubMed: 33852846]

16. Mittag J, Winterhager E, Bauer K, Grummer R, Congenital hypothyroid female pax8-deficient mice are infertile despite thyroid hormone replacement therapy. Endocrinology 148, 719–725 (2007); published online EpubFeb (10.1210/en.2006-1054). [PubMed: 17082261]

17. Mayran A, Pelletier A, Drouin J, Pax factors in transcription and epigenetic remodelling. Semin Cell Dev Biol 44, 135–144 (2015); published online EpubAug (10.1016/j.semcdb.2015.07.007). [PubMed: 26234816]

18. Chaves-Moreira D, Morin PJ, Drapkin R, Unraveling the Mysteries of PAX8 in Reproductive Tract Cancers. Cancer Res 81, 806–810 (2021); published online EpubFeb 15 (10.1158/0008-5472.CAN-20-3173). [PubMed: 33361393]

19. Laury AR, Perets R, Piao H, Krane JF, Barletta JA, French C, Chirieac LR, Lis R, Loda M, Hornick JL, Drapkin R, Hirsch MS, A comprehensive analysis of PAX8 expression in human epithelial tumors. Am J Surg Pathol 35, 816–826 (2011); published online EpubJun (10.1097/PAS.0b013e318216c112). [PubMed: 21552115]

20. Perets R, Wyant GA, Muto KW, Bijron JG, Poole BB, Chin KT, Chen JY, Ohman AW, Stepule CD, Kwak S, Karst AM, Hirsch MS, Setlur SR, Crum CP, Dinulescu DM, Drapkin R, Transformation of the fallopian tube secretory epithelium leads to high-grade serous ovarian cancer in Brca;Tp53;Pten models. Cancer Cell 24, 751–765 (2013); published online EpubDec 9 (10.1016/j.ccr.2013.10.013). [PubMed: 24332043]

21. Maniati E, Berlato C, Gopinathan G, Heath O, Kotantaki P, Lakhani A, McDermott J, Pegrum C, Delaine-Smith RM, Pearce OMT, Hirani P, Joy JD, Szabova L, Perets R, Sansom OJ, Drapkin R, Bailey P, Balkwill FR, Mouse Ovarian Cancer Models Recapitulate the Human Tumor Microenvironment and Patient Response to Treatment. Cell Rep 30, 525–540 e527 (2020); published online EpubJan 14 (10.1016/j.celrep.2019.12.034). [PubMed: 31940494]

22. Di Palma T, Filippone MG, Pierantoni GM, Fusco A, Soddu S, Zannini M, Pax8 has a critical role in epithelial cell survival and proliferation. Cell Death Dis 4, e729 (2013); published online EpubJul 18 (10.1038/cddis.2013.262). [PubMed: 23868062]

23. Ghannam-Shahbari D, Jacob E, Kakun RR, Wasserman T, Korsensky L, Sternfeld O, Kagan J, Bublik DR, Aviel-Ronen S, Levanon K, Sabo E, Larisch S, Oren M, Hershkovitz D, Perets R, PAX8 activates a p53-p21-dependent pro-proliferative effect in high grade serous ovarian carcinoma. Oncogene 37, 2213–2224 (2018); published online EpubApr (10.1038/s41388-017-0040-z). [PubMed: 29379162]

24. Rodgers LH, O. h. E, Young AN, Burdette JE, Loss of PAX8 in high-grade serous ovarian cancer reduces cell survival despite unique modes of action in the fallopian tube and ovarian surface epithelium. Oncotarget 7, 32785–32795 (2016); published online EpubMay 31 (10.18632/oncotarget.9051). [PubMed: 27129161]

25. Elias KM, Emori MM, Westerling T, Long H, Budina-Kolomets A, Li F, MacDuffie E, Davis MR, Holman A, Lawney B, Freedman ML, Quackenbush J, Brown M, Drapkin R, Epigenetic remodeling regulates transcriptional changes between ovarian cancer and benign precursors. JCI Insight 1, (2016); published online EpubAug 18 (10.1172/jci.insight.87988).

26. Corona RI, Seo JH, Lin X, Hazelett DJ, Reddy J, Fonseca MAS, Abassi F, Lin YG, Mhawech-Fauceglia PY, Shah SP, Huntsman DG, Gusev A, Karlan BY, Berman BP, Freedman ML, Gayther SA, Lawrenson K, Non-coding somatic mutations converge on the PAX8 pathway in ovarian cancer. Nat Commun 11, 2020 (2020); published online EpubApr 24 (10.1038/s41467-020-15951-0). [PubMed: 32332753]

27. Garcia-Heredia JM, Verdugo Sivianes EM, Lucena-Cacace A, Molina-Pinelo S, Carnero A, Numb-like (NumbL) downregulation increases tumorigenicity, cancer stem cell-like properties and resistance to chemotherapy. Oncotarget 7, 63611–63628 (2016); published online EpubSep 27 (10.18632/oncotarget.11553). [PubMed: 27613838]

28. Allen HF, Wade PA, Kutateladze TG, The NuRD architecture. Cell Mol Life Sci 70, 3513–3524 (2013); published online EpubOct (10.1007/s00018-012-1256-2). [PubMed: 23340908]

29. Grimley E, Liao C, Ranghini EJ, Nikolovska-Coleska Z, Dressler GR, Inhibition of Pax2 Transcription Activation with a Small Molecule that Targets the DNA Binding Domain. ACS Chem Biol 12, 724–734 (2017); published online EpubMar 17 (10.1021/acschembio.6b00782). [PubMed: 28094913]
30. De Palma M, Biziato D, Petrova TV, Microenvironmental regulation of tumour angiogenesis. Nat Rev Cancer 17, 457–474 (2017); published online EpubAug (10.1038/nrc.2017.51). [PubMed: 28706266]
31. Fishilevich S, Nudel R, Rappaport N, Hadar R, Plaschkes I, Iny Stein T, Rosen N, Kohn A, Twik M, Safran M, Lancet D, Cohen D, GeneHancer: genome-wide integration of enhancers and target genes in GeneCards. Database (Oxford) 2017, (2017); published online EpubJan 1 (10.1093/database/bax028).
32. Zhou H, Yang YH, Basile JR, Characterization of the Effects of Semaphorin 4D Signaling on Angiogenesis. Methods Mol Biol 1493, 429–441 (2017)10.1007/978-1-4939-6448-2_31). [PubMed: 27787869]
33. Zhou H, Yang YH, Binmadi NO, Proia P, Basile JR, The hypoxia-inducible factor-responsive proteins semaphorin 4D and vascular endothelial growth factor promote tumor growth and angiogenesis in oral squamous cell carcinoma. Exp Cell Res 318, 1685–1698 (2012); published online EpubAug 15 (10.1016/j.yexcr.2012.04.019). [PubMed: 22652457]
34. Adler EK, Corona RI, Lee JM, Rodriguez-Malave N, Mhawech-Fauceglia P, Sowter H, Hazelett DJ, Lawrenson K, Gayther SA, The PAX8 cistrome in epithelial ovarian cancer. Oncotarget 8, 108316–108332 (2017); published online EpubDec 12 (10.18632/oncotarget.22718). [PubMed: 29312534]
35. Lawrenson K, Fonseca MAS, Liu AY, Segato Dezem F, Lee JM, Lin X, Corona RI, Abbasi F, Vavra KC, Dinh HQ, Gill NK, Seo JH, Coetzee S, Lin YG, Pejovic T, Mhawech-Fauceglia P, Rowat AC, Drapkin R, Karlan BY, Hazelett DJ, Freedman ML, Gayther SA, Noushmehr H, A Study of High-Grade Serous Ovarian Cancer Origins Implicates the SOX18 Transcription Factor in Tumor Development. Cell Rep 29, 3726–3735 e3724 (2019); published online EpubDec 10 (10.1016/j.celrep.2019.10.122). [PubMed: 31825847]
36. Shi K, Yin X, Cai MC, Yan Y, Jia C, Ma P, Zhang S, Zhang Z, Gu Z, Zhang M, Di W, Zhuang G, PAX8 regulon in human ovarian cancer links lineage dependency with epigenetic vulnerability to HDAC inhibitors. Elife 8, (2019); published online EpubMay 3 (10.7554/eLife.44306).
37. Bohm M, Wachtel M, Marques JG, Streiff N, Laubscher D, Nanni P, Mamchaoui K, Santoro R, Schafer BW, Helicase CHD4 is an epigenetic coregulator of PAX3-FOXO1 in alveolar rhabdomyosarcoma. J Clin Invest 126, 4237–4249 (2016); published online EpubNov 1 (10.1172/JCI85057). [PubMed: 27760049]
38. Grimm D, Bauer J, Wise P, Kruger M, Simonsen U, Wehland M, Infanger M, Corydon TJ, The role of SOX family members in solid tumours and metastasis. Semin Cancer Biol, (2019); published online EpubMar 23 (10.1016/j.semcancer.2019.03.004).
39. Hou L, Srivastava Y, Jauch R, Molecular basis for the genome engagement by Sox proteins. Semin Cell Dev Biol 63, 2–12 (2017); published online EpubMar (10.1016/j.semcdb.2016.08.005). [PubMed: 27521520]
40. Wilson M, Koopman P, Matching SOX: partner proteins and co-factors of the SOX family of transcriptional regulators. Curr Opin Genet Dev 12, 441–446 (2002); published online EpubAug ([PubMed: 12100890]
41. Lang D, Epstein JA, Sox10 and Pax3 physically interact to mediate activation of a conserved c-RET enhancer. Hum Mol Genet 12, 937–945 (2003); published online EpubApr 15 (10.1093/hmg/ddg107). [PubMed: 12668617]
42. Mascarenhas JB, Littlejohn EL, Wolsky RJ, Young KP, Nelson M, Salgia R, Lang D, PAX3 and SOX10 activate MET receptor expression in melanoma. Pigment Cell Melanoma Res 23, 225–237 (2010); published online EpubApr (10.1111/j.1755-148X.2010.00667.x). [PubMed: 20067553]
43. Zhang S, Bell E, Zhi H, Brown S, Imran SAM, Azuara V, Cui W, OCT4 and PAX6 determine the dual function of SOX2 in human ESCs as a key pluripotent or neural factor. Stem Cell Res Ther 10, 122 (2019); published online EpubApr 18 (10.1186/s13287-019-1228-7). [PubMed: 30999923]
44. Ooki A, Dinalankara W, Marchionni L, Tsay JJ, Goparaju C, Maleki Z, Rom WN, Pass HI, Hoque MO, Epigenetically regulated PAX6 drives cancer cells toward a stem-like state via GLI-

SOX2 signaling axis in lung adenocarcinoma. Oncogene 37, 5967–5981 (2018); published online EpubNov (10.1038/s41388-018-0373-2). [PubMed: 29980786]

45. Reddy J, Fonseca MAS, Corona RI, Nameki R, Dezem FS, Klein IA, Chang H, Chaves-Moreira D, Afeyan L, Malta TM, Lin X, Abbasi F, Font-Tello A, Sabedot T, Cejas P, Rodríguez-Malavé N, Ji-Heui Seo D-CL, Matulonis U, Karlan BY, Gayther SA, Gusev A, Noushmehr H, Long H, Freedman ML, Drapkin R, Abraham BJ, Young RA, Lawrenson K, Predicting master transcription factors from pan-cancer expression data. bioRxiv 839142, (2019)10.1101/839142).
46. Yang H, Lee S, Lee S, Kim K, Yang Y, Kim JH, Adams RH, Wells JM, Morrison SJ, Koh GY, Kim I, Sox17 promotes tumor angiogenesis and destabilizes tumor vessels in mice. J Clin Invest 123, 418–431 (2013); published online EpubJan (10.1172/JCI64547). [PubMed: 23241958]
47. Devy L, Blacher S, Grignet-Debrus C, Bajou K, Masson V, Gerard RD, Gils A, Carmeliet G, Carmeliet P, Declerck PJ, Noel A, Foidart JM, The pro- or antiangiogenic effect of plasminogen activator inhibitor 1 is dose dependent. FASEB J 16, 147–154 (2002); published online EpubFeb (10.1096/fj.01-0552com). [PubMed: 11818362]
48. Stefansson S, Petitclerc E, Wong MK, McMahon GA, Brooks PC, Lawrence DA, Inhibition of angiogenesis in vivo by plasminogen activator inhibitor-1. J Biol Chem 276, 8135–8141 (2001); published online EpubMar 16 (10.1074/jbc.M007609200). [PubMed: 11083866]
49. Stefansson S, Lawrence DA, The serpin PAI-1 inhibits cell migration by blocking integrin alpha V beta 3 binding to vitronectin. Nature 383, 441–443 (1996); published online EpubOct 3 (10.1038/383441a0). [PubMed: 8837777]
50. Wu J, Strawn TL, Luo M, Wang L, Li R, Ren M, Xia J, Zhang Z, Ma W, Luo T, Lawrence DA, Fay WP, Plasminogen activator inhibitor-1 inhibits angiogenic signaling by uncoupling vascular endothelial growth factor receptor-2-alphaVbeta3 integrin cross talk. Arterioscler Thromb Vasc Biol 35, 111–120 (2015); published online EpubJan (10.1161/ATVBAHA.114.304554). [PubMed: 25378411]
51. Vargesson N, Thalidomide-induced teratogenesis: history and mechanisms. Birth Defects Res C Embryo Today 105, 140–156 (2015); published online EpubJun (10.1002/bdrc.21096). [PubMed: 26043938]
52. Bleu M, Mermet-Meillon F, Apfel V, Barys L, Holzer L, Bachmann Salvy M, Lopes R, Amorim Monteiro Barbosa I, Delmas C, Hinniger A, Chau S, Kaufmann M, Haenni S, Berneiser K, Wahle M, Moravec I, Vissieres A, Poetsch T, Ahrne E, Carte N, Voshol J, Bechter E, Hamon J, Meyerhofer M, Erdmann D, Fischer M, Stachyra T, Freuler F, Gutmann S, Fernandez C, Schmelzle T, Naumann U, Roma G, Lawrenson K, Nieto-Oberhuber C, Cobos-Correa A, Ferretti S, Schubeler D, Galli GG, PAX8 and MECOM are interaction partners driving ovarian cancer. Nat Commun 12, 2442 (2021); published online EpubApr 26 (10.1038/s41467-021-22708-w). [PubMed: 33903593]
53. Karst AM, Drapkin R, Primary culture and immortalization of human fallopian tube secretory epithelial cells. Nat Protoc 7, 1755–1764 (2012); published online EpubSep (10.1038/nprot.2012.097). [PubMed: 22936217]
54. Sen P, Lan Y, Li CY, Sidoli S, Donahue G, Dou Z, Frederick B, Chen Q, Luense LJ, Garcia BA, Dang W, Johnson FB, Adams PD, Schultz DC, Berger SL, Histone Acetyltransferase p300 Induces De Novo Super-Enhancers to Drive Cellular Senescence. Mol Cell 73, 684–698 e688 (2019); published online EpubFeb 21 (10.1016/j.molcel.2019.01.021). [PubMed: 30773298]
55. Cox J, Mann M, MaxQuant enables high peptide identification rates, individualized p.p.b.-range mass accuracies and proteome-wide protein quantification. Nat Biotechnol 26, 1367–1372 (2008); published online EpubDec (10.1038/nbt.1511). [PubMed: 19029910]
56. Reddy J, Fonseca MAS, Corona RI, Nameki R, Segato Dezem F, Klein IA, Chang H, Chaves-Moreira D, Afeyan LK, Malta TM, Lin X, Abbasi F, Font-Tello A, Sabedot T, Cejas P, Rodriguez-Malave N, Seo JH, Lin DC, Matulonis U, Karlan BY, Gayther SA, Pasaniuc B, Gusev A, Noushmehr H, Long H, Freedman ML, Drapkin R, Young RA, Abraham BJ, Lawrenson K, Predicting master transcription factors from pan-cancer expression data. Sci Adv 7, eabf6123 (2021); published online EpubNov 26 (10.1126/sciadv.abf6123). [PubMed: 34818047]

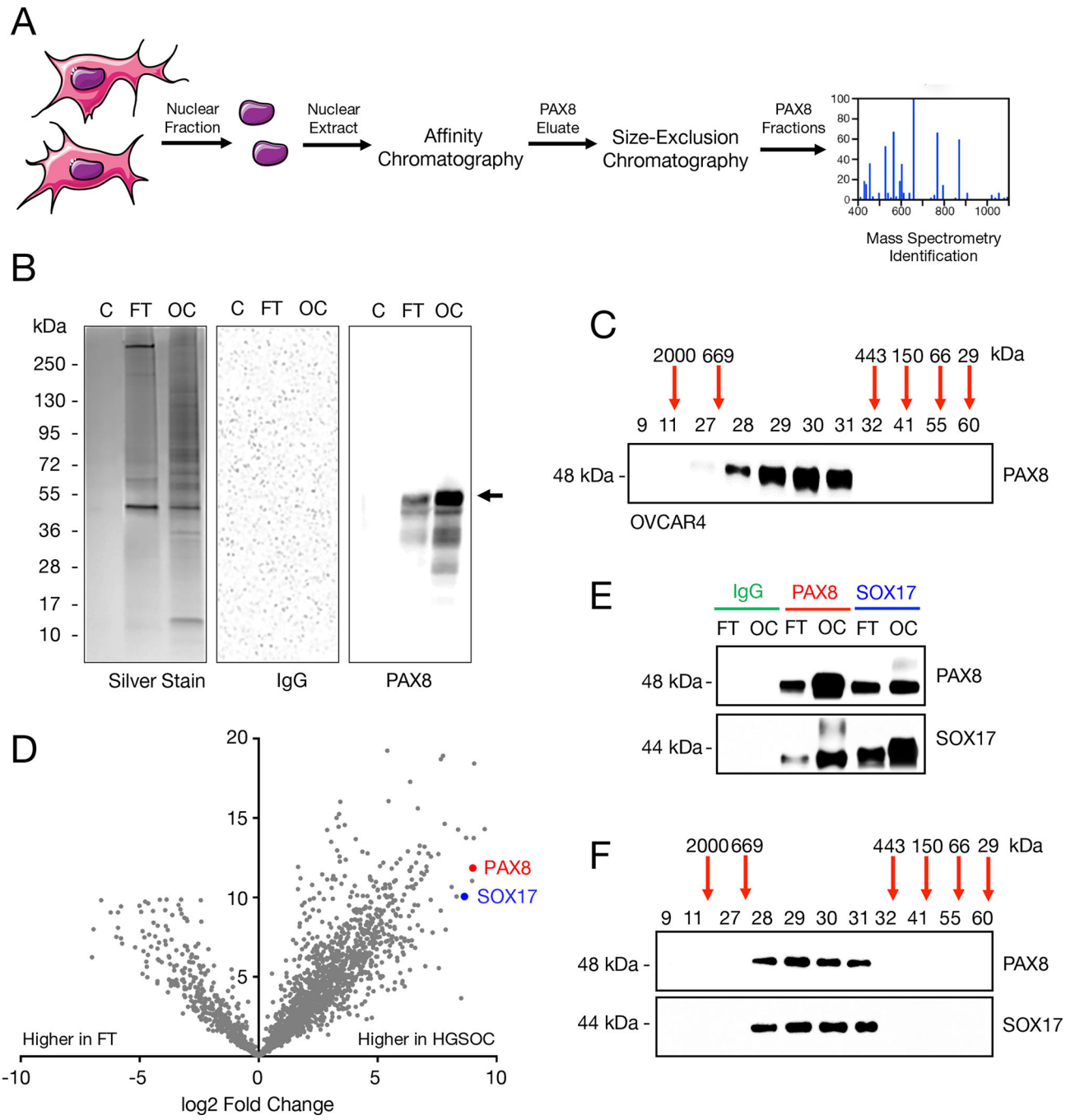

Fig. 1. Three-step proteomic approach identifies putative PAX8-interacting partners.

(A) Schematic of the workflow for the PAX8-interacting partner identification. **(B)** Representative examples of endogenous PAX8 immunoprecipitation from fallopian tube secretory cell line FT194 (lane “FT”) and HGSOC line OVCAR4 (lane “OC”) detected by silver staining and immunoblotting. IMR90 cells, which are PAX8-negative, were used as negative control (lane “C”). The arrow indicates migration of full-length PAX8. **(C)** Representative immunoblot of size-exclusion fractions for PAX8 in OVCAR4 cells. **(D)** PAX8 immunoprecipitates and gel-filtration fractions shown in (B and C) were analyzed by

mass spectrometry to identify PAX8-interacting partners. The results are shown as a Volcano plot, displayed as interacting proteins detected in greater amounts in isolates from fallopian tube cells than those from HGSOCs, and vice-versa. Plot shows averaged data from all 3 HGSOC cell lines (OVCAR4, KURAMOCHI, and OVSAHO) and all 3 fallopian tube cell lines (FT194, FT246, and FT282). **(E)** Assessment of PAX8 and SOX17 interaction by co-immunoprecipitation assay in lysates from FT194 (FT) and OVCAR4 (OC) cell lines. **(F)** Immunoblotting for PAX8 and SOX17 in size-exclusion fractions to assess co-elution in OVCAR4 cells. Blots in (B, C, E, and F) show a representative of 3 OC and 3 FT cell lines independently assessed.

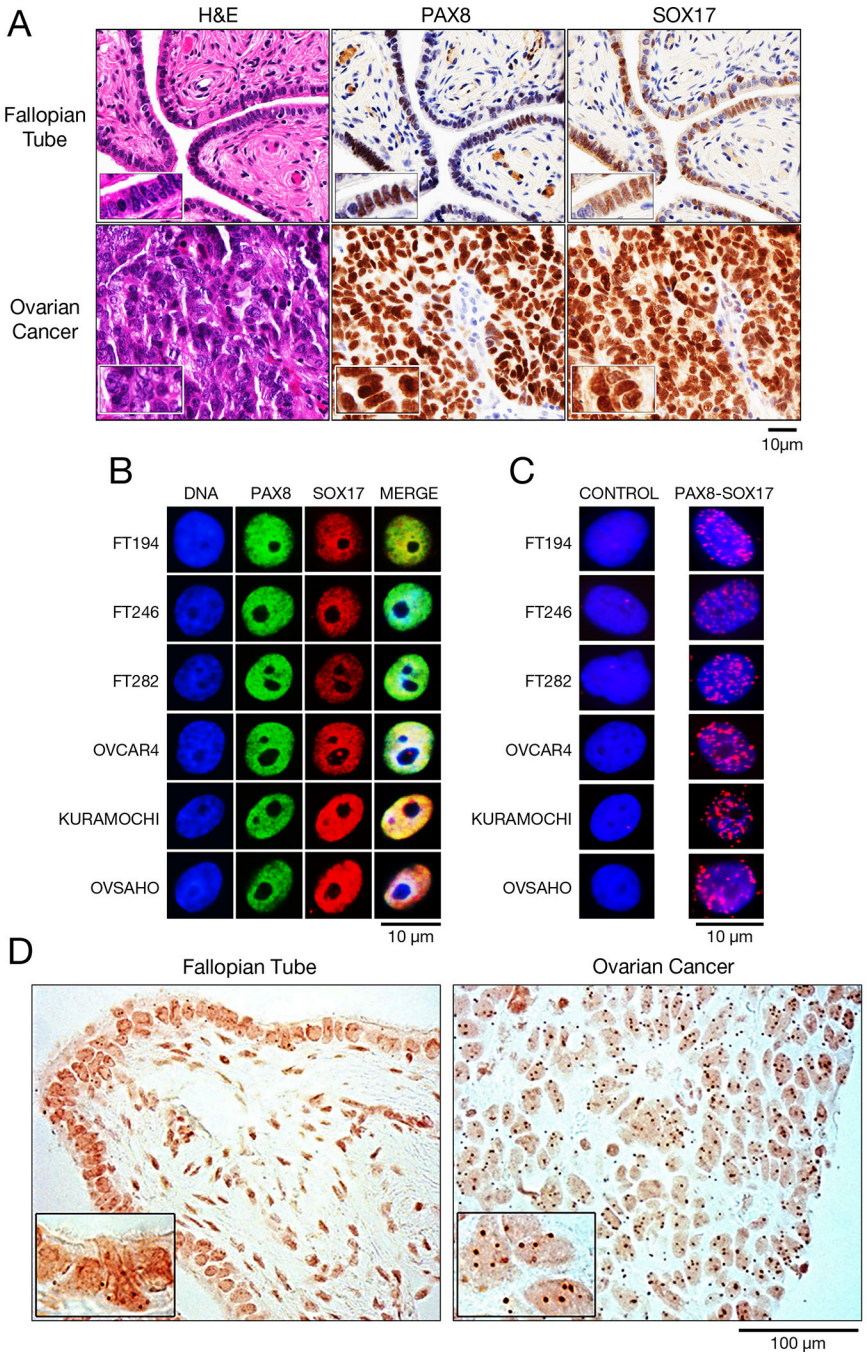

Fig. 2. PAX8 physically interacts with SOX17 in human fallopian tube and ovarian cancer tissues.

(A) Immunohistochemistry showing nuclear co-expression of PAX8 and SOX17 in FTSEC and HGSOC cells. 5 different benign FT samples and 5 different ovarian cancer patient samples were analyzed, and one representative case of each is shown. Scale bar, 10μm. **(B and C)** Immunofluorescence (B) and PLA (C) assessing co-localization of PAX8 and SOX17 in secretory cells (FT194, FT246, and FT282) and carcinoma cells (OVCAR4, KURAMOCHI, and OVSAHO). Scale bar, 10μm. The nuclei were acquired in one z-plane

with 60X magnification. Images are representative of duplicate experiments, 100 cells analyzed in each. **(D)** In situ PLA signals (dark brown puncta) in normal fallopian tube sections and HGSOC samples. Nuclei are visible as light brown in the background and were acquired in one z-plane with 40x magnification. These experiments were performed on the same 10 cases from (A), and representative sections are shown. Scale bar, 100μm.

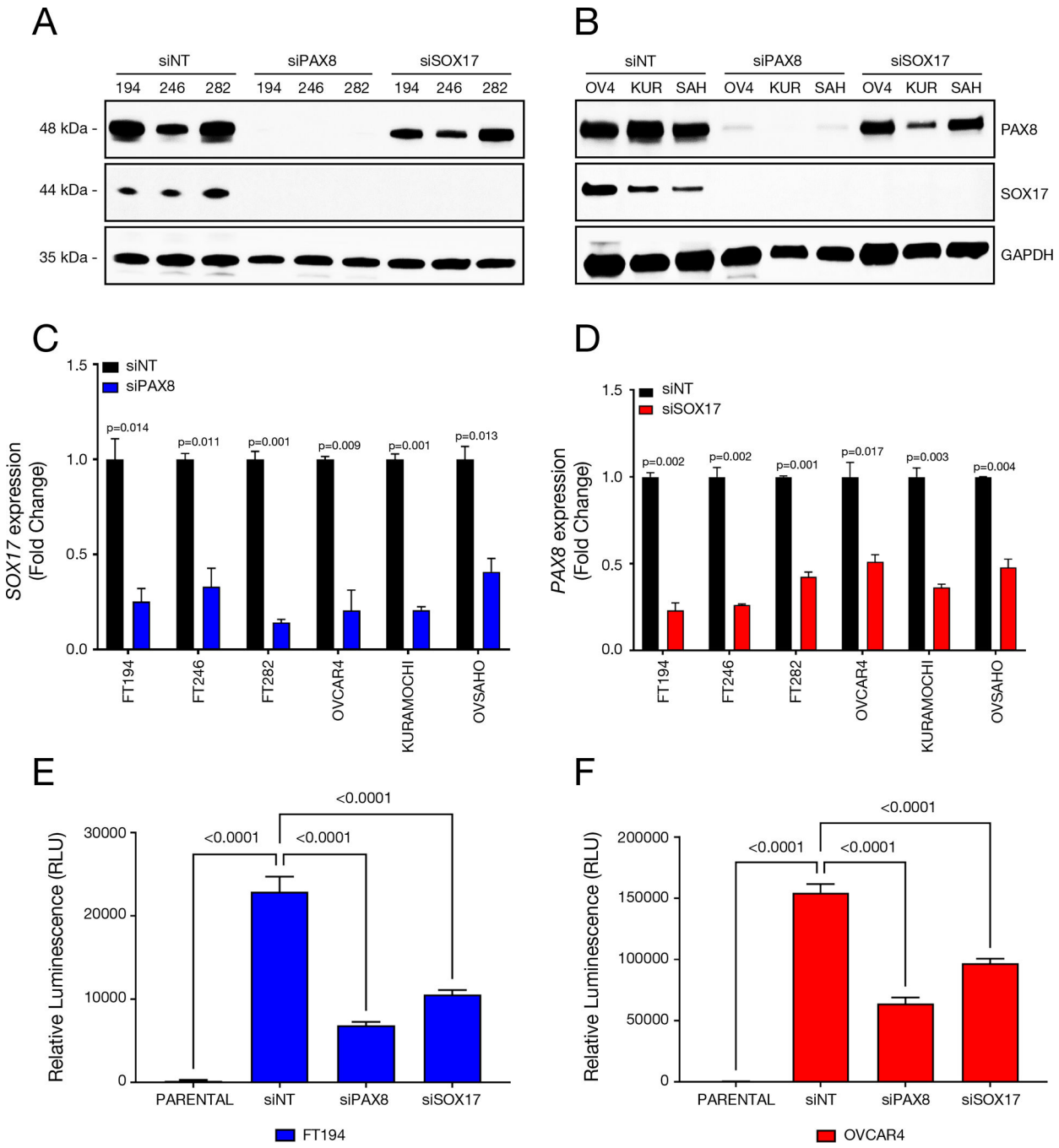

Fig. 3. PAX8 and SOX17 are mutually regulated.

(A and B) Immunoblot analyses for PAX8 or SOX17 after each protein's knockdown in three different FTSEC and three different HGSOC cells. A representative blot of three independent experiments is shown, and these results are representative of those obtained in three FTSEC (FT194, FT246, and FT282) and three HGSOC (OVCAR4, KURAMOCHI, and OVSAHO) lines. **(C and D)** Real-time PCR analysis following knockdown of PAX8 or SOX17 in FTSEC (FT194, FT246, and FT282) and in HGSOC (OVCAR4, KURAMOCHI, and OVSAHO) cells depicting the transcriptional co-regulation of SOX17 by PAX8. Data

are means ± S.D. from 3 independent experiments in each cell line. **(E and F)** Luciferase reporter assay using vector containing 5X PAX8-recognition sequence in cells with or without PAX8 or SOX17 knockdown. Data are shown for OVCAR4 and FT194, means ± S.D. from three independent experiments done in triplicate. *P*-values by unpaired t-tests (C and D) and one-way ANOVA analysis (E and F).

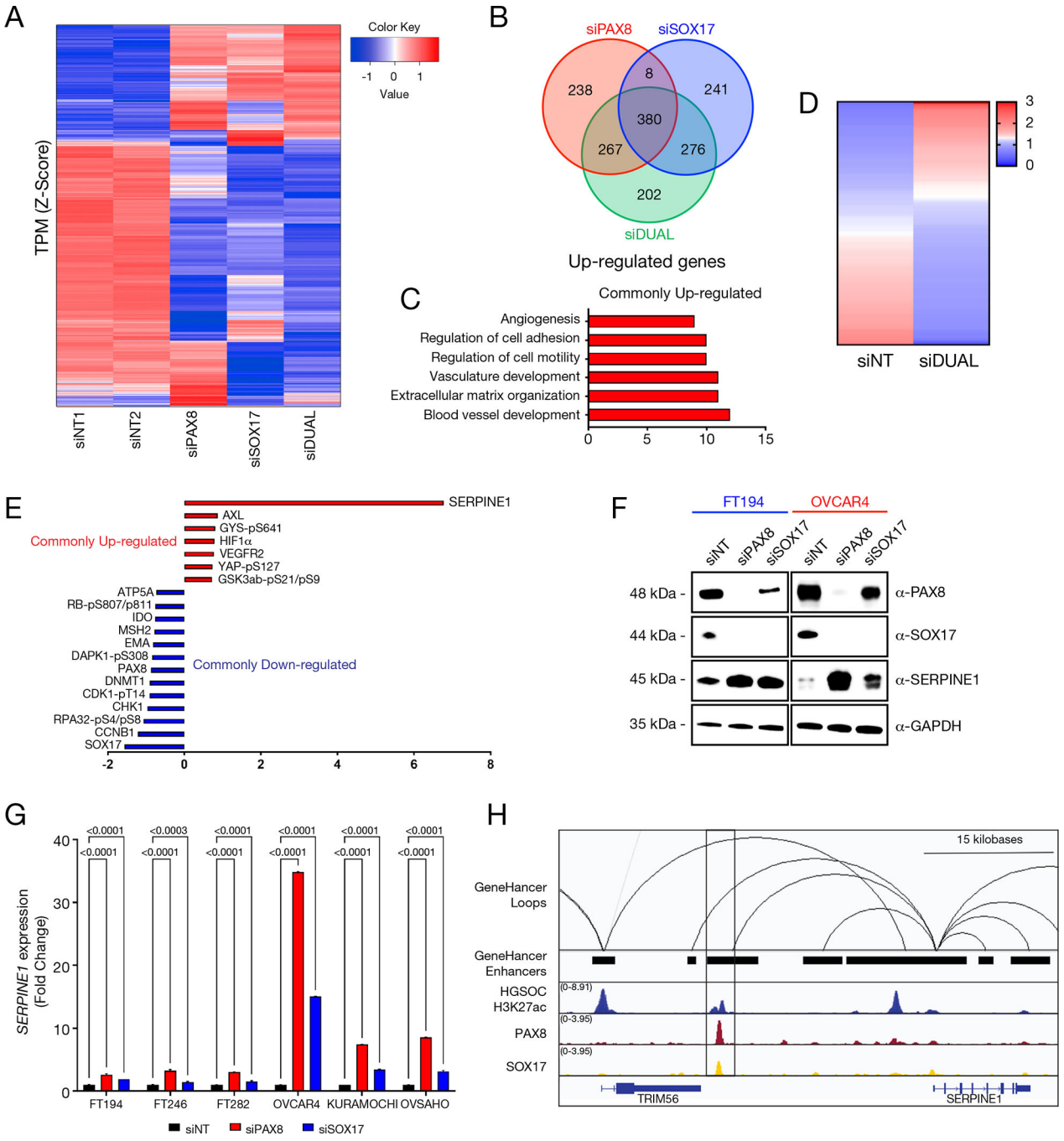

Fig. 4. PAX8 and SOX17 regulate a common set of genes.

(A) RNA-seq unsupervised gene clustering in OVCAR4 cells 72-hours after knockdown of PAX8, SOX17, or both (siDUAL), or incubation with 2 non-targeted siRNA controls (siNT1 and siNT2), each done in duplicate. Fold change >1; $P < 0.05$. **(B)** Venn diagram showing the number of genes for which expression was increased under each condition. Genes are specified within table S1. **(C)** Ontology analysis of the PAX8-SOX17 commonly up-regulated genes. **(D)** RPPA unsupervised clustering of PAX8-SOX17 commonly regulated proteins in OVCAR4 cells after PAX8, SOX17, or dual knockdown. Proteins are listed in

table S2. **(E)** Top-ranked PAX8-SOX17 commonly regulated proteins. Data in (D and E) are from 3 independent experiments in OVCAR4 done in triplicate. **(F)** Immunoblot showing SERPINE1 up-regulation after PAX8 or SOX17 knockdown in HGSOC and FTE cell lines. Results are shown for OVCAR-4 and FT194, as representative of 3 lines each. **(G)** Real-time PCR showing *SERPINE1* up-regulation after PAX8 or SOX17 knockdown in the 6 indicated cell lines. *P* values are indicated, by ANOVA analysis. **(H)** ChIP-seq analysis of PAX8 and SOX17 binding in the *SERPINE1* gene region. Interacting enhancers are shown, as predicted by GeneHancer.

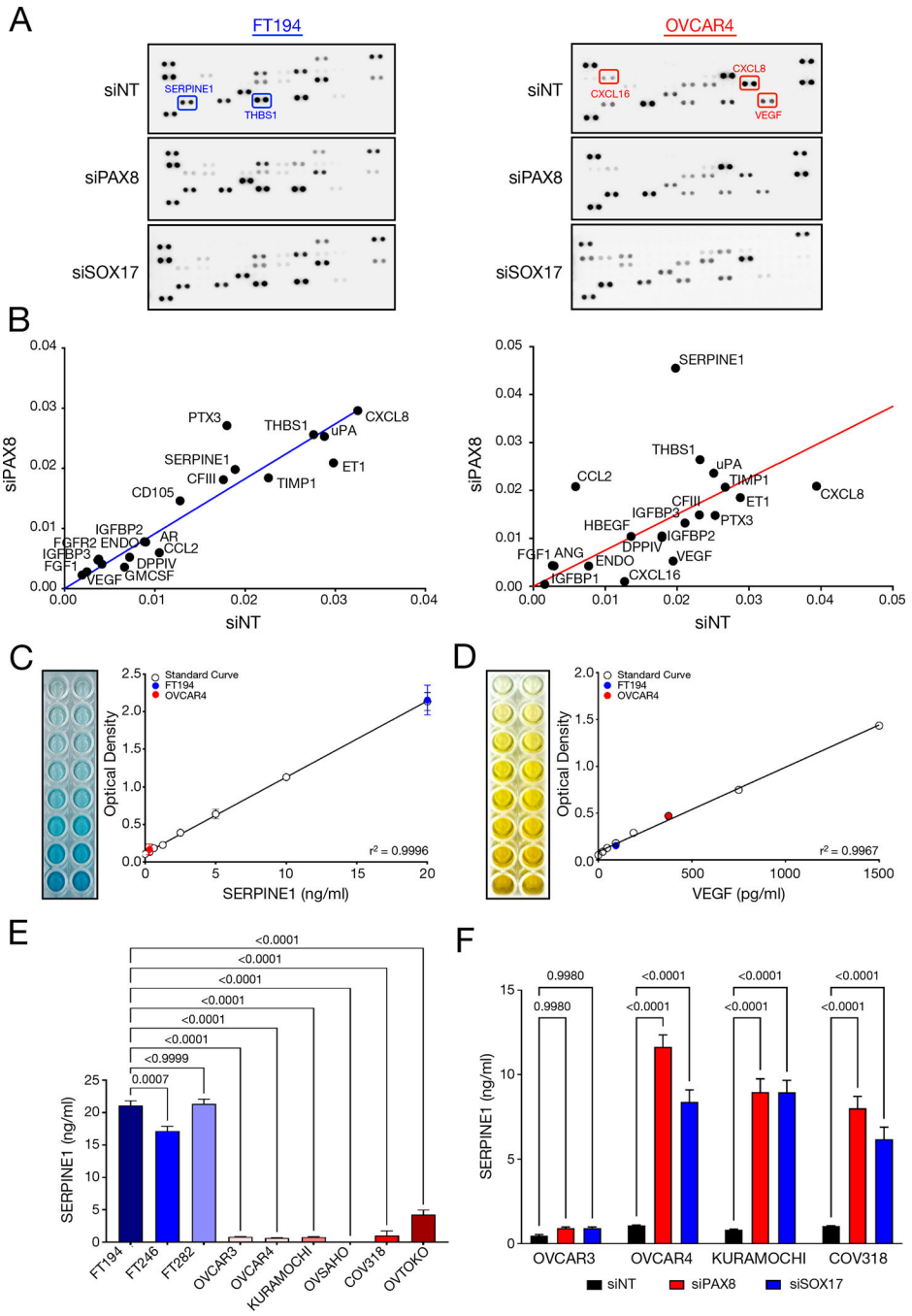

Fig. 5. PAX8 and SOX17 regulate the secretion of angiogenesis mediators.

(A) Human angiogenesis array of conditioned media from FT194 and OVCAR4 cells following PAX8 or SOX17 knockdown. **(B)** Effect of PAX8 knockdown on specific analytes was produced by quantifying the array membrane spots intensity. **(C and D)** ELISA for quantification of secreted SERPINE1 (C) and VEGF (D) in the FT194- and OVCAR4-conditioned media. **(E)** ELISA showing SERPINE1 secreted by FTSEC and HGSOC. **(F)** ELISA experiments showing the effects of PAX8 or SOX17 knockdown on levels of SERPINE1 in HGSOC. Data in (E and F) are means and SD from three independent

experiments done in duplicate. In (A and B), representative data from FT194 and OVCAR4 cells are shown, as one of three experiments in each cell line done in triplicate. In (C and D), representative data from FT194 and OVCAR4 are shown (done in duplicate in each cell line). In (E and F), representative data from cell lines are shown, from three experiments each in duplicate; *P*-values by one-way ANOVA analysis.

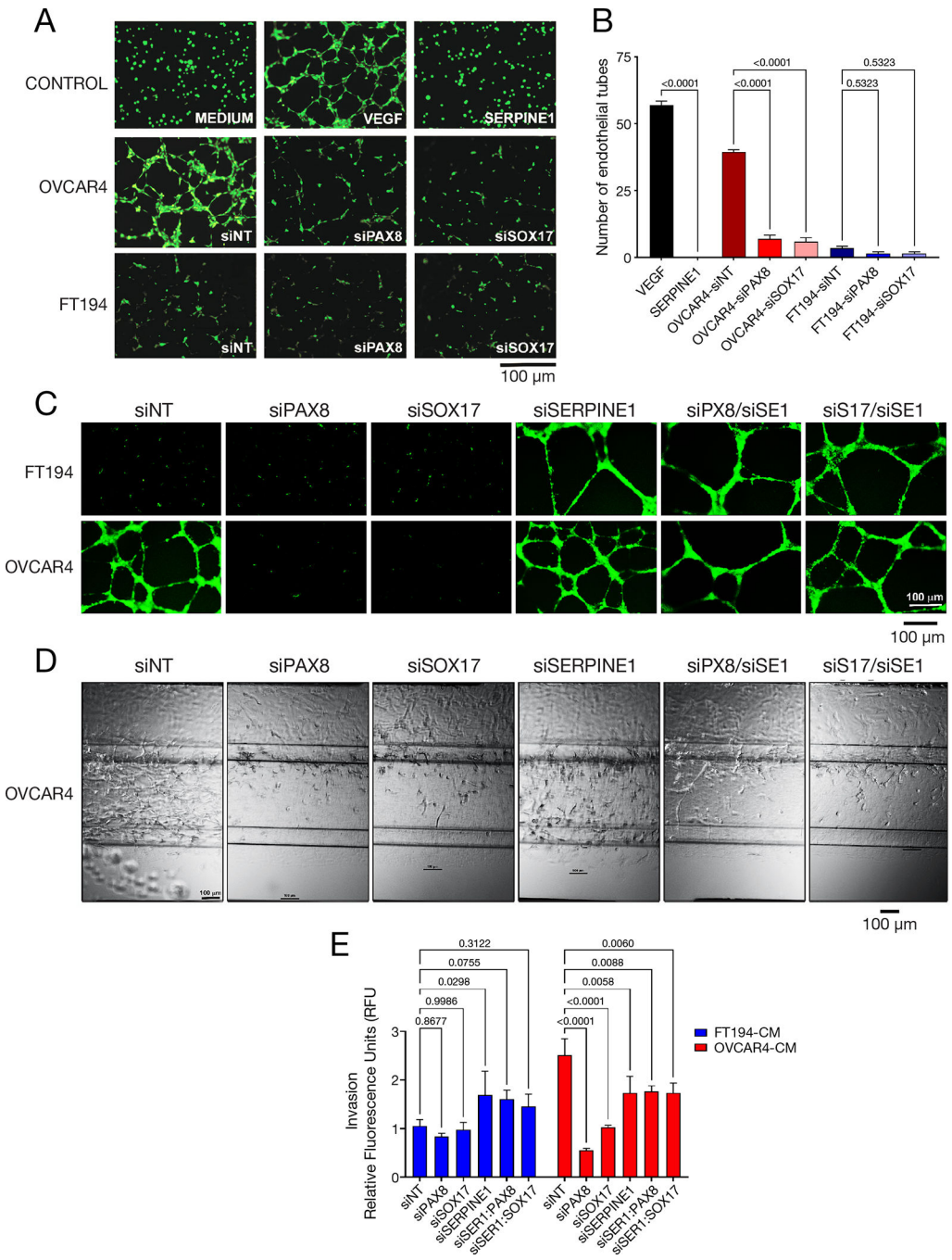

Fig. 6. PAX8 and SOX17 promote ovarian cancer angiogenesis.

(A) Tube formation assay in HUVECs after culture with recombinant VEGF, recombinant SERPINE1, and conditioned media from FT194 or OVCAR4 cells with and without PAX8 or SOX17 knockdown. Images are representative of experiments done in triplicate. Scale bar, 100 µm. **(B)** Quantitation of the HUVEC neo-vessels loops from (A). Data are three different experiments done in triplicate. **(C)** Endothelial cells tube formation after treatment with conditioned media from FT194 and OVCAR4 cells with the following knockdowns: PAX8, SOX17, SERPINE1, dual SERPINE1 + PAX8, or dual SERPINE1 + SOX17. Images

are representative of three independent experiments. **(D)** 3D angiogenic sprouting seven days after the addition of conditioned media from OVCAR4 cells in which PAX8, SOX17, SERPINE1, or a combination (PX8, PAX8; S17, SOX17; SE1, SERPINE1) were knocked down. Images are representative of three independent experiments done in triplicate. **(E)** Invasion by endothelial cells in the presence of conditioned media from FT194 or OVCAR4 cells with the indicated knockdowns. Data are mean and SD from three experiments done in triplicate. *P*-values noted in (B) and (E) were obtained by one-way ANOVA analysis.

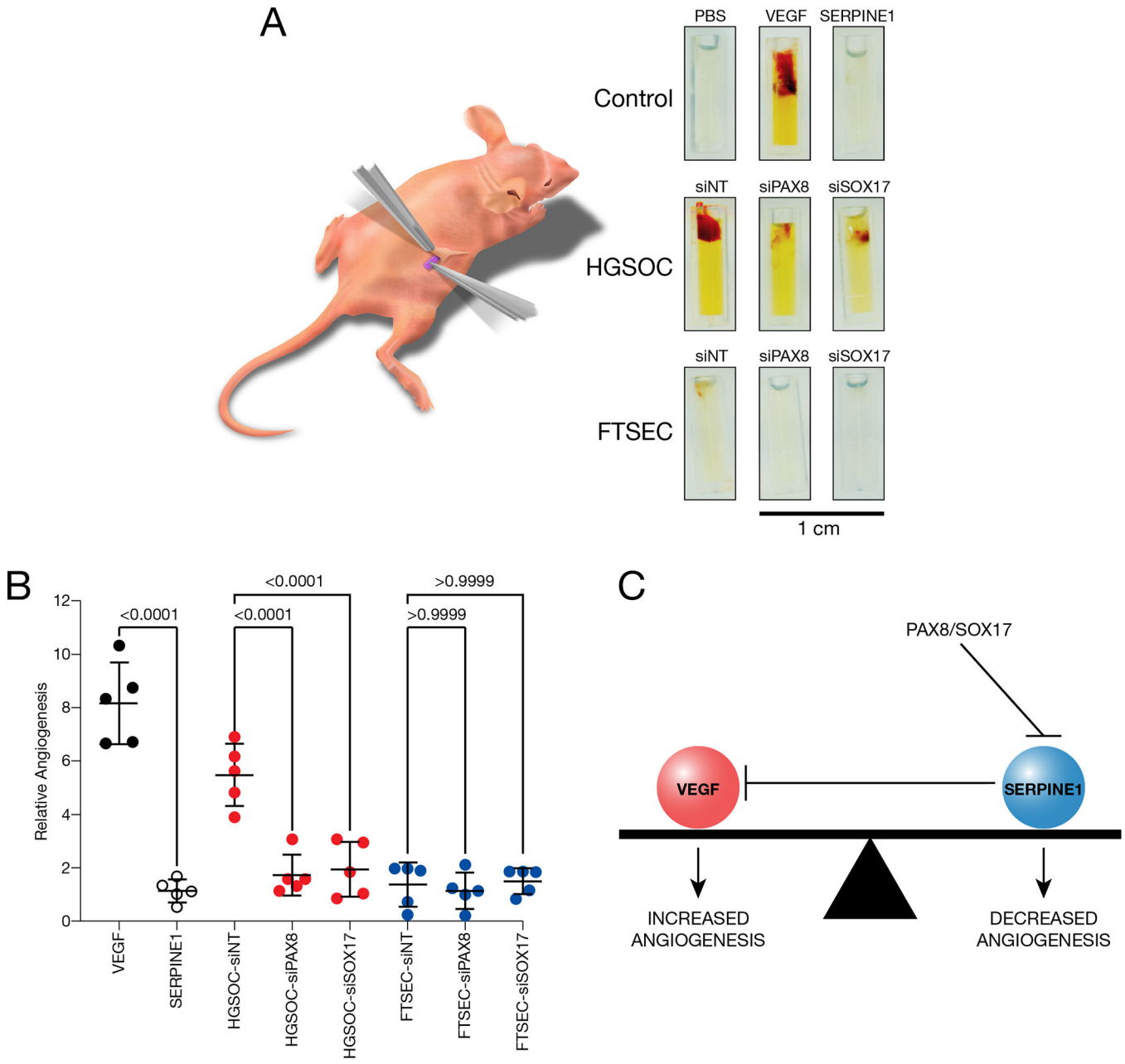

Fig. 7. PAX8 and SOX17 promote ovarian cancer-directed angiogenesis in vivo.

(A) Neovascularization is observed in angioreactors containing conditioned media from HGSOC (OVCAR4) cells, but not from FTSEC (FT194) after implantation in nude mice. **(B)** Quantitation of host endothelial cell invasion into angioreactors. In (A and B), n= 5 mice per group. *P*-values are indicated, by one-way ANOVA analysis. **(C)** Proposed model wherein suppression of SERPINE1 expression by PAX8-SOX17 in the malignant state enables unfettered angiogenesis by VEGF and other pro-angiogenic factors.

Table 1:

Putative PAX8-interacting partners.

UniProtKB Accession no.	Spot name	Description	Theoretical mass (kDa)	MaxQuant search results			Log Fold change Cancer *vs.* Normal[#]
				No. of matched peptides	Sequence coverage (%)	Score	
TRANSCRIPTION FACTORS AND REGULATORS							
Q06710	PAX8	Paired box protein 8	48.2	13	33.8	162.9	+1.38
Q13263	TRIM28	Transcription intermediary factor 1-β	88.5	5	11.3	79.4	−0.22
Q1MSW8	TP53	Cellular tumor antigen p53	50.2	4	22.2	76.1	+2.79
Q9H6I2	SOX17	Transcription factor SOX17	44.3	3	11.1	74.8	+1.05
P78347	GTF2I	General transcription factor III	107.9	19	11.3	73.3	+1.06
Q86YP4	GATAD2A	Transcriptional repressor p66-alpha	68.1	7	9.6	45.1	−0.66
P40763	STAT3	Signal transducer and activator of transcription 3	76.1	8	3.9	39.6	+0.01
A5YKK6	CNOT1	CCR4-NOT transcription complex subunit 1	266.4	6	2.5	38.1	−1.13
P17480	UBTF	Nucleolar transcription factor 1	75.9	10	6.3	31.6	−0.96
P51532	SMARCA4	Transcription activator BRG1	184.6	15	3.9	28.8	−0.18
O00268	TAF4	Transcription initiation factor TFIID subunit 4	50.2	3	6.8	20.4	+0.70
O60885	BRD4	Bromodomain-containing protein 4	152.2	3	2.5	18.7	−2.08
Q13573	SNW1	SNW domain-containing protein 1	43.3	3	9.9	18.1	+1.57
O75448	MED24	Mediator of RNA polymerase II transcription subunit 24	91.3	3	4.6	17.8	−0.79
Q9NZN8	CNOT2	CCR4-NOT transcription complex subunit 2	29.9	2	9.1	16.7	−0.97
P20290	BTF3	Transcription factor BTF3	17.7	2	17.3	14.6	+2.02
A0A0U1RRM1	GATAD2B	Transcriptional repressor p66-β	63.4	4	5.9	14.2	−0.30
E9PJZ4	MED17	Mediator of RNA polymerase II transcription subunit 17	16.3	2	16.1	13.8	+1.94
Q96EI5	TCEAL4	Transcription elongation factor A protein-like 4	21.5	5	11.8	12.5	0.00
H3BQQ2	ZNF598	Zinc finger protein 598	93.3	4	1.5	12.5	+0.34
Q9NYF8	BCLAF1	Bcl-2-associated transcription factor 1	52.9	11	5.4	12.2	−0.23
O75175	CNOT3	CCR4-NOT transcription complex subunit 3	31.2	8	16.3	10.9	−4.48
Q4FD37	ZNF148	Zinc finger protein 148	74.5	4	1.2	9.2	0.00

UniProtKB Accession no.	Spot name	Description	Theoretical mass (kDa)	MaxQuant search results			Log Fold change Cancer *vs.* Normal[#]
				No. of matched peptides	Sequence coverage (%)	Score	
Q96AQ6	PBXIP1	Pre-B-cell leukemia transcription factor-interacting protein 1	57.5	6	2.2	8.5	+0.65
P42224	STAT1	Signal transducer and activator of transcription 1-alpha/beta	88.3	3	1.7	8.1	−0.93
Q9ULX9	MAFF	Transcription factor MafF	14.5	2	11.9	7.5	0.00
Q13127	REST	RE1-silencing transcription factor	52.2	3	2.1	7.3	+1.02
P46937	YAP1	Transcriptional coactivator YAP1	18.7	9	6.5	6.6	+1.27
P53999	SUB1	Activated RNA polymerase II transcriptional coactivator p15	14.4	3	18.9	6.4	+1.90
P40424	PBX1	Pre-B-cell leukemia transcription factor 1	46.6	1	10.3	5.8	+0.78
P18846	ATF1	Cyclic AMP-dependent transcription factor ATF-1	57.6	23	5.8	2.1	+0.03
RNA PROCESSING							
Q9BQ02	NCL	Nucleolin	76.6	11	30.1	188.9	−0.63
A8K849	ZFR	Zinc finger RNA-binding protein	66.3	3	7.1	16.6	+0.41
Q9NVP1	DDX18	ATP-dependent RNA helicase DDX18	61.6	4	4.4	13.9	+2.24
Q59FS7	DDX24	ATP-dependent RNA helicase DDX24	75.1	1	1.6	8.4	+5.29
Q9Y2W2	WBP11	WW domain-binding protein 11	64.9	1	2.4	7.2	+0.93
DNA PROCESSING							
P33993	MCM7	DNA replication licensing factor MCM7	81.2	11	23.8	114.6	+0.35
Q92878	RAD50	DNA repair protein RAD50	138.4	12	11.5	85.4	+0.49
Q9Y265	RUVBL1	RuvB-like 1	50.2	8	25.4	76.1	+1.46
Q14839	CHD4	Chromodomain-helicase-DNA-binding protein 4	215.2	15	3.6	45.8	+0.18
Q9P258	RCC2	Protein RCC2	56.1	5	14.2	43.2	+1.53
Q9Y230	RUVBL2	RuvB-like 2	51.1	9	13.2	35.4	+0.84
P49736	MCM2	DNA replication licensing factor MCM2	87.4	6	6.1	26.2	−0.09
P18887	XRCC1	DNA repair protein XRCC1	42.8	2	5.8	13.5	−1.03
B7Z8C6	DBF4	Protein DBF4 homolog A	51.8	2	3.1	6.5	+1.75
EPIGENETIC REGULATORS							
Q09028	RBBP4	Histone-binding protein RBBP4	46.9	4	7.9	27.9	−2.96
O94776	MTA2	Metastasis-associated protein MTA2	75.0	3	3	12.5	+0.03

UniProtKB Accession no.	Spot name	Description	Theoretical mass (kDa)	MaxQuant search results			Log Fold change Cancer *vs.* Normal[#]
				No. of matched peptides	Sequence coverage (%)	Score	
Q6IT96	HDAC1	Histone deacetylase	55.1	2	4.4	11.8	+1.99
Q96L91	EP400	E1A-binding protein p400	335.8	1	0.6	9.4	+0.31
Q8TEK3	DOT1L	Histone-lysine N-methyltransferase, H3 lysine-79 specific	24.1	3	3.4	7.6	−1.60
Q9UPP1	PHF8	Histone lysine demethylase PHF8	33.2	1	4.5	7.2	−0.27
Q13330	MTA1	Metastasis-associated protein MTA1	28.7	8	5.1	6.3	+1.55
Q59G93	BRD1	Bromodomain-containing protein 1	53.8	1	1.9	6.2	+0.30
APOPTOTIC SIGNALING PATHWAY							
Q8N163	CCAR2	Cell cycle and apoptosis regulator protein 2	102.9	8	10.2	57.1	+0.51
Q8IX12	CCAR1	Cell division cycle and apoptosis regulator protein 1	131.4	5	3.1	30.9	+1.56
Q9BZZ5	API5	Apoptosis inhibitor 5	37.5	4	10.0	27.2	+2.22
Q9UKV3	ACIN1	Apoptotic chromatin condensation inducer in the nucleus	122.5	3	3.8	19.9	−2.24
D6RC06	HINT1	Histidine triad nucleotide-binding protein 1	7.3	1	21.5	6.7	+0.84
TRANSFORMATION SIGNALING PATHWAY							
G3XAM7	CTNNA1	Catenin α-1	92.7	6	8.8	76.4	−1.01
B4DSW9	CTNNB1	Catenin β-1	77.5	3	3.9	24.3	+0.13
O00499	BIN1	Myc box-dependent-interacting protein 1	43.2	1	3.6	6.3	−1.12

Nuclear extracts from FT194, FT246, FT282, OVCAR4, KURAMOCHI, and OVSAHO cells were utilized for affinity-purification of PAX8 before fractionation on a Sephacryl S-300 column. PAX8-enriched fractions from the column were subjected to mass spectrometry to identify PAX8-associated proteins.

[#]Average log fold differences between PAX8-associated proteins in the cancer relative to normal cells (+, higher in cancer; −, higher in normal).